MOLECULAR MECHANISMS OF γ-ORYZANOL

AGAINST NON-SMALL CELL LUNG CANCER

A THESIS SUBMITTED TO THE GRADUATE DIVISION OF THE UNIVERSITY OF HAWAIʻI AT MĀNOA IN PARTIAL FULFILLMENT OF THE REQUIREMENTS FOR THE DEGREE OF

MASTER OF SCIENCE

IN

MOLECULAR BIOSCIENCES AND BIOENGINEERING

DECEMBER 2016

by

Sofía Doello Román

Thesis Committee:

Qing X. Li (Chairperson)
Jon-Paul Bingham
Yong-Soo Kim

A mis padres, Loli y Antonio,
por su apoyo incondicional y
confianza, incluso desde el
otro lado del mundo.

ACKNOWLEDGEMENT

I would like to express my gratitude to my supervisor, Dr. Qing Li, for giving me the opportunity to work in his lab and for being always supportive. I would like to thank the Fulbright Commission, for making possible my graduate studies in the United States. Additionally, I would like to thank the Rural Development Administration from Korea for funding this research project.

I would like to thank my committee members, Dr. Jon-Paul Bingham and Dr. Yong-Soo Kim, for their valuable comments and guidance throughout the completion of this work. I would like to show my appreciation to Dr. Il Kyu Cho for sharing his ideas with me and helping me getting started, and Dr. Jung Bong Kim, for providing me with the natural products necessary to carry out this study. I would also like to thank Dr. Nicholas James, for allowing me to use his tissue culture facilities, and his students, Bethany Sanstrum and Brandee Goo, for sharing their space with me.

I would like to thank all Dr. Li's lab members for creating a very professional and collegial working environment. I would especially like to thank Dr. Margaret Baker, Dr. Zhen Cao, Camila Ortega, and Zhibin Liang for the inspiring conversations and their useful advice.

Finally, I would like to express my gratitude to the University of Hawai'i at Mānoa and the Molecular Biosciences and Bioengineering Department for making this program possible.

Thank you.

Sofia Doello

ABSTRACT

Non-small cell lung cancer (NSCLC) is the most common type of lung cancer, which is the leading cause of cancer death, with an increasing prevalence every year. Specific treatments for some of the multiple kinds of NSCLC have been developed, but their efficacy is low and they are not applicable to all types. Cell viability experiments suggested that rice bran oil could be a source of anti-carcinogenic phytochemicals against NSCLC. γ-Oryzanol is the major component in rice bran oil and has anti-cancer properties on various prostate cancer cell lines and in some animal models. The goal of this study was to determine whether the most abundant components in the γ-oryzanol mixture (24-mCAF, CAF, CMF and β-SF) have cytotoxic activity against A549 cells, a NSCLC cell line.

The effect of these compounds on cell proliferation was tested using the colorimetric methylthiazol tetrazolium (MTT) assay. Among all four compounds, 24-mCAF showed the strongest inhibitory effect on cell proliferation of A549 cells, while β-SF did not seem to affect it.

An iTRAQ-based quantitative proteomics analysis combined with Ingenuity Pathway Analysis (IPA) revealed that the changes in the proteome caused by 24-mCAF were consistent with cancer inhibition. Cell death and apoptosis were activated and cell proliferation was inactivated. Myb binding protein 1A is a tumor suppressor protein that binds to several transcription factors. The results obtained in this study indicate that 24-mCAF induces MYBBP1A up-regulation, which contributes to stop cancer progression through different mechanisms. These mechanisms include its interaction with P53, which induces apoptosis and cell cycle arrest; its interaction with NFκB, which inhibits inflammatory processes; and its interaction with SIRT6, which regulates the expression of several cancer-related proteins. Up-regulation of MYBBP1A by 24-mCAF was verified with western blot and the results were consistent with those obtained with iTRAQ. This study provides the first step for understanding the effect of γ-oryzanol on A459 cells at the cellular and molecular level, providing a possible candidate for NSCLC treatment or prevention.

TABLE OF CONTENTS

LIST OF TABLES

LIST OF FIGURES

LIST OF ABBREVIATIONS

24-m CAF	24-methylenecyloartanyl ferulate
5-LOX	5-lipoxygenase-5
ACN	Acetonitrile
AKT	Protein kinase B
ATCC	American Type Culture Collection
β-SF	Beta sitosteryl ferulate
BAEC	Bovine aortic endothelial cells
BSA	Bovine serum albumin
CAF	Cycloartenyl ferulate
CMF	Campesteryl ferulate
COP-II	Coat protein complex 2
COX-2	Cyclooxygenase 2
DHPN	2,20-dihydroxy-di-n-propyl- nitrosamine
DMAB	3,20-dimethyl-4-aminobiphenyl
DMEM	Dulbecco's Modified Eagle Medium
DMSO	Dimethyl sulfoxide
ECI1	Enoyl-CoA delta isomerase 1
EDTA	Ethylenediaminetetraacetic acid
EGFR	Epidermal growth factor receptor
EHEN	N-ethyl-N-hydroxyethyl-nitrosamine
ER	Endoplasmic reticulum
EPO	Erythropoietin
FBS	Fetal bovine serum
HIF	Hypoxia inducible factor
FH	Fumarate hydratase
GDP	Guanosine diphosphate
GC/MS	Gas chromatography - mass spectrometry
GLUT-1	Glucose transporter protein 1
GTP	Guanosine triphophate
HPLC	High performance liquid chromatography
IPA	Ingenuity pathway analysis

iTRAQ	Isobaric tags for relative and absolute quantification
KRAS	Kirsten rat sarcoma
LC-MS/MS	Liquid chromatography – tandem mass spectrometry
MAPK	Mitogen-activated protein kinase
MEK	Mitogen-activated protein kinase kinase
MDH1	Malate dehydrogenase
MGF	Mascot generic file
mTOR	Mammalian target of rapamycin
MTT	Methylthiazol tetrazolim
MYBBP1A	Myb binding protein 1A
NAD	Nicotinamide adenine dinucleotide
NADP	Nicotinamide adenine dinucleotide phosphate
NDUFB9	NADH dehydrogenase ubiquinone 1 beta subcomplex subunit 9
NFκB	Nuclear factor kappa-light-chain-enhancer of activated B cells
NSCLC	Non-small cell lung cancer
P13K	Phosphoinositide 3-kinase
P53	Tumor protein 53
PDGF	Platelet derived growth factor
PVDF	Polyvinylidene difluoride
RAS	Rat sarcoma
SDS-PAGE	Sodium dodecyl sulfate polyacrylamide gel electrophoresis
SCX	Strong cation exchange chromatography
SIRT-6	Sirtuin 6
STAT	Signal transducer and activator of transcription protein
TBST	Tris-buffered saline tween-20
TKI	Tyrosine kinase inhibitor
TPD52	Tumor protein D52
UGGT1	UPD-glucose glycoprotein glucosyltransferase 1
VEGF	Vascular endothelial growth factor

CHAPTER I. INTRODUCTION

1.1. Lung cancer

Lung cancer is by far the leading cause of cancer death in both men and women. In 2016, lung and bronchus cancer are expected to cause 27% of the cancer deaths in males and 26% in women in the United States. It is the second most commonly diagnosed cancer, accounting for 14% of the new cases. The prevalence of this type of cancer keeps increasing worldwide each year (American Cancer Society, 2016; Jemal et al., 2009).

Non-small cell lung cancer (NSCLC) is the most common type of lung cancer, representing about 85% of the cases. The two most commonly mutated oncogenes in NSCLC are the epidermal growth factor receptor (*EGFR*) and Kirsten rat sarcoma (*KRAS*). Mutations in these two genes are mutually exclusive in NSCLC. When EGFR is overexpressed, it causes cells to grow in a faster and uncontrolled way (Figure 1). Erlotinib and gefitinib are epidermal growth factor receptor tyrosine kinase inhibitors (EGFR-TKIs) that block the signal from the overexpressed EGFR and that are used as a treatment for NSCLC. *KRAS* encodes a GTPase downstream of EGFR which signals through the PI3K/AKT/mTOR and STAT pathways involved in cell survival, and the RAS/ RAF/MEK/MAPK pathway involved in cell proliferation; its mutation also results in uncontrolled growth. Cells presenting *KRAS* mutations are not sensitive to treatment with TKIs like the drugs mentioned above. General cancer treatments, such as surgery, chemotherapy and radiotherapy, are usually applied to NSCLC patients with *KRAS* mutations, since there is no targeted therapy available (Krypuy et al., 2006; Riely et al., 2009).

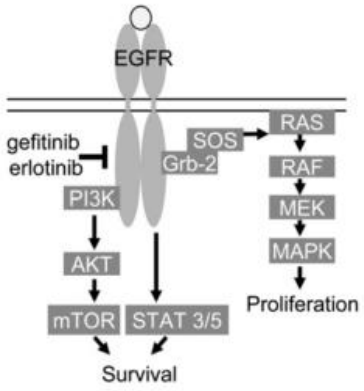

Figure 1. Simplified schematic of EGFR and KRAS signaling pathways. Adapted from Riely et al., 2009.

KRAS mutations occur in approximately 33% of NSCLCs and the prognosis of this type of cancer is very poor. KRAS is one of the most difficult drug targets due to its picomolar affinity for GTP/GDP and the absence of known allosteric regulatory sites. When it is mutated GTP hydrolysis is impaired, which results in the increase of the proportion of active GTP-bound KRAS. Although some KRAS inhibitors have been reported in the past few years, the design of a drug remains a big challenge. There is a great need for the development and implementation of a novel, effective and affordable treatment for this kind of cancer (Ostrem et al., 2013).

1.2. Rice bran oil as a source of anti-carcinogenic phytochemicals.

Plant extracts have been widely used in traditional medicine for centuries. Nowadays, the use of bioactive phytochemicals is gaining attention due to their low cost, low toxicity, high tolerability and reported biological activities. Several phytochemicals, such as reservatrol, curcumin, capsaicin and genistein have been associated with anti-carcinogenic activity and protective role against side effects of conventional chemotherapeutic agents (Pal et al., 2016; Goyal et al., 2016).

Rice bran oil is an important byproduct of rice milling industry that is gaining commercial importance because of its health benefits. Although rice bran oil has a similar fatty acid profile than other oils, it contains hundreds of bioactive compounds that are responsible for its antioxidant activity, cholesterol lowering capacity and anti-cancer effects (Sohail et al., 2016). These properties have been extensively studied during the last years. Dapar et al., (2013) showed that the bran oil from IR64 rice has cytotoxic activity against A549 lung adenocarcinoma epithelial cells, a NSCLC cell line that carries KRAS mutations. This finding suggests that some of the bioactive phytochemicals from rice bran oil might be good candidates for prevention or treatment of NSCLC.

1.3. Composition of rice bran oil

Rice bran constitutes 6% of a rice kernel and includes pericarp, seed coat, nucellus, aleurone and soft germ of a rice seed (Figure 1). Approximately 15-20% of the bran is oil and around 4% of this oil is unsaponifiable material, which is a relatively large proportion compared to other vegetable oils. The unsaponifiable material is mainly constituted by γ-oryzanol (1-3% w/w) and vitamin E derivatives (tocopherols and tocotrienols). γ-Oryzanol is the bioactive component of rice bran oil that has shown the most beneficial properties. It was initially

thought to be a single component, but it is actually a complex mixture of different ferulate esters of triterpene alcohols and plant sterols. 24-methylenecyloartanyl ferulate (24-mCAF), cycloartenyl ferulate (CAF), campesteryl ferulate (CMF) and β-sitosteryl ferulate (β-SF) are the most abundant compounds in γ-oryzanol, contributing to about 94% of the total mass (Table1; Figure 2) (Patel et al., 2004; Britz et al., 2007; Kim et al., 2015).

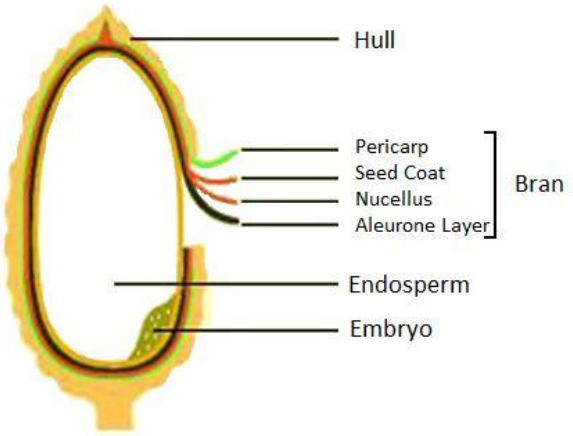

Figure 2. Rice kernel structure adapted from Huang et al., 2003.

Table 1. Most represented compounds in γ-oryzanol

Name	Abbreviation	% of total mass
24-methylenecycloartanyl ferulate	24-mCAF	23 - 42
Cycloartenyl ferulate	CAF	10 - 41
Campesteryl ferulate	CMF	8 – 20
β-sitosteryl ferulate	β-SF	7 - 14

Kim et al., 2013

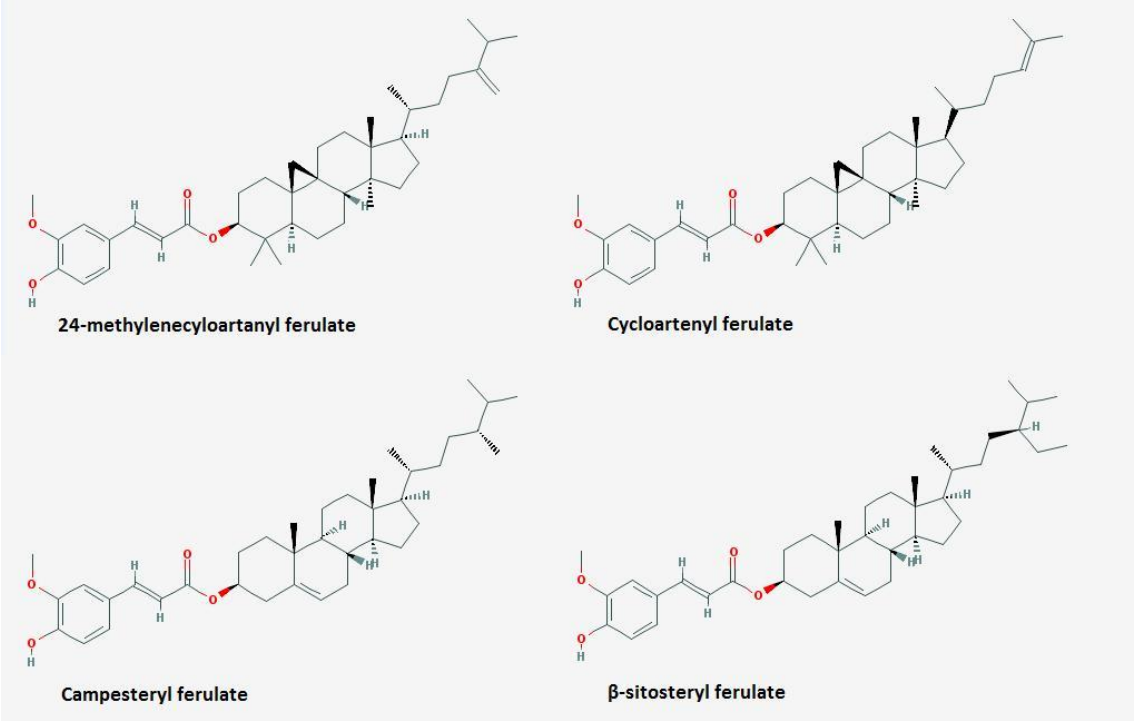

Figure 3. Structure of the most represented compounds in γ-oryzanol. Kim et al., 2015.

1.4. Beneficial properties of γ-oryzanol

Numerous studies have reported the beneficial properties of γ-oryzanol, which was first known as an antioxidant compound. Xu et al. (2001) used accelerated oxidation of linoleic acid to test the antioxidant activity of 24-mCAF, CAF and CMF. Linoleic acid is easily oxidized because it contains 1,4-pentadiene, which is very vulnerable to free radical attack. Its oxidation can be determined by measuring the production of linoleic acid hydroperoxides. All three compounds significantly reduced the rate of hydroperoxides production. Their results suggest that the antioxidant activity of these compounds come from the ferulate portion of the molecule, since the proportions of different linoleic acid hydroperoxides obtained with each of the three components are similar to the one obtained with ferulic acid (Xu et al., 2001).

Another important property of γ-oryzanol is its cholesterol lowering capacity. Several studies on humans and animals showed that γ-oryzanol lowers low density lipoprotein and serum total cholesterol levels by influencing absorption of dietary cholesterol in the intestine. During digestion, steryl ferulates are thought to be cleaved into ferulic acid and free sterols by intestinal enzymes. The released free sterols inhibit the absorption of cholesterol into the systemic circulation (Mandak et al., 2004).

γ-Oryzanol also possesses anti-inflammatory activity mainly due to NF-κB inhibition. Inflammatory responses typically require NF-κB translocation into the nucleus. Sakai et al. (2012) studied the effect of γ-oryzanol in NF-κB translocation in bovine aortic endothelial cells (BAECs) and found that a treatment of 30 μM for 16 hours considerably inhibited the translocation. The inhibitory effect of γ-oryzanol was higher than the observed with pyrrolidine dithiocarbamate (PDTC), a synthetic antioxidant known as a NF-κB inhibitor, at the same concentration.

The synthesis and release of dopamine and norepinephrine in the medial basal hypothalamic region of the rat brain were increased by γ-oryzanol. These molecules are hypothalamic neurotransmitters that influence the synthesis and release of hormones in the pituitary (Wheeler et al. 1991). Treatment with 300 mg of γ-oryzanol administered orally produced a significant reduction of the elevated serum thyroid-stimulating hormone levels produced by the pituitary in hypothyroid patients (Patel et al., 2004). An intravenous injection of 5 mg γ-oryzanol to male rats remarkably decreased the levels of luteinizing hormone released by the pituitary. This effect might be beneficial in the management of menopause symptoms (Wheeler et al., 1991).

Several studies have reported the anti-cancer properties of γ-oryzanol. Klongpityapong et al. (2013) showed that γ-oryzanol significantly inhibits cell growth on the prostate cancer cell lines DU145 and PC3, and that it down-regulates the expression of the catalase and glutathione peroxidase genes. These genes are both important in protecting the cell from oxidative damage and their down-regulation can lead to cell death. Hirsch et al. (2015) reported that this compound decreases cell viability by activating apoptosis and blocking cell cycle progression at G2/M in PC3 cells and at G0/G1 in DU145 cells. In addition, they found that genes CAV-1, important for cell proliferation, and PCGEM1, involved in apoptosis inhibition, were down-regulated after treatment with γ-oryzanol in PC3 and DU145 cells, respectively. Kim et al. (2012) investigated the effect of γ-oryzanol and other rice bran oil components on tumor growth in mice. After administering the compounds in the diet for 2 weeks, animals were inoculated with CT-26 colon cancer cells and they were treated for 2 more weeks. Tumors from animals treated with γ-oryzanol showed significantly less growth than tumors from the control mice. Tumor inhibition was associated with increased cytolytic activity of splenic natural killer cells, partial restoration of nitric oxide production and phagocytosis in peritoneal macrophages, increased levels of pro-inflammatory cytokines released from macrophages, reduced number of blood vessels inside the tumor, and reduction

of the expression of vascular endothelial growth factor (VEGF), cyclooxy-genase-2 (COX-2) and 5-lipoxygenase-5 (5-LOX). These findings suggest that γ-oryzanol may inhibit neoangiogenesis inside the tumors (Szcześniak et al., 2015).

1.5. Absorption and metabolism of γ-oryzanol

The absorption of plant sterols is generally limited; approximately only 5% of ingested plant sterols are absorbed. Fujiwara et al. (1983) administered γ-oryzanol-^{14}C orally to rats and found that, after 72 hours, 9.8% radioactivity was found in the urine and 84.5% in the feces, which indicates that absorption of γ-oryzanol was very poor (Huang et al., 2003).

Huang et al. (2003) studied the digestibility of γ-oryzanol using an *in vitro* model that includes pepsin, bile and pancreatin (a mixture of pancreatic enzymes containing lipase, amylase, protease, cholesterol esterase and other enzymes) solutions. They tested the effect of these enzymes on γ-oryzanol in crystalline and micellar form. Their results show that γ-oryzanol concentration decreases after peptic and pancreatic digestion, especially when it is in micellar form, probably because when it is in crystalline form it is less accessible for the enzymes. CMF and β-SF decreased more obviously than other γ-oryzanols after incubation with pancreatic enzymes, which indicates that they may be more susceptible to digestion. This may be due to the similarity of their chemical structure with cholesterol (Figure 3). Unlike other γ-oryzanols, they do not have methyl groups in their ring structures and the side chains have only an extra methyl group difference at C-24 position for CMF and an extra ethyl group for β-SF in comparison with cholesterol. Further analysis of the digestion products of γ-oryzanol with GC/MS revealed that the amount of free sterols increased, supporting the hypothesis that γ-oryzanols are hydrolyzed by pancreatic enzymes at the ester bond, releasing free sterols and ferulic acid. However, ferulic acid was not detected, which suggests that it is further degraded (Huang et al., 2003).

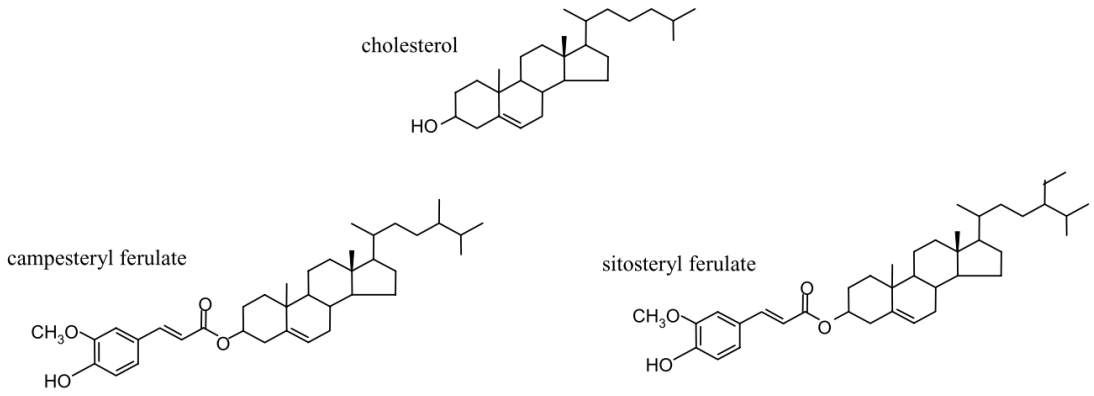

Figure 4. Chemical structures of cholesterol, campesteryl ferulate and sitosteryl ferulate

1.6. Toxicity of γ-oryzanol

Toxicity of γ-oryzanol has been tested in different organisms. Induction of carcinogenesis in mice was studied by administering 2 g/kg body weight/day γ-oryzanol in the diet of B6C3F1 mice for 78 weeks. Tumor incidence seemed not to be different between the control and treated animals, indicating that γ-oryzanol is not toxic for B6C3F1 mice (Huang et al., 2003).

Additionally, Sakai et al. (2012) tested the cytotoxic effect of γ-oryzanol on bovine aortic endothelial cells (BAECs). After treatment with 30 μM γ-oryzanol for 24 hours, no influence in the percentage of viable cells compared to vehicle-treated cells was observed.

Moreover, only negative results were obtained when the mutagenic effect of γ-oryzanol was investigated using the *Bacillus subtilis* Rec assay (bacterial DNA repair test), Ames test (bacterial reverse mutation test), rat bone marrow chromosome aberration test, and metabolic cooperation inhibition test using Chinese hamster V79 cell.

In contrast to the results mentioned above, Hirose et al. (1998) reported carcinogenesis enhancing effect of γ-oryzanol on the lungs of F344 rats. However, this effect was weak and occurred only at very high dose. Animals were treated with 3 different carcinogens (2,20-dihydroxy-di-*n*-propyl- nitrosamine (DHPN), *N*-ethyl-*N*-hydroxyethyl-nitrosamine (EHEN) and 3,20-dimethyl-4-aminobiphenyl (DMAB)) for 3 weeks and then were treated with γ-oryzanol in their basal diet for 32 weeks. Increase in the multiplicity of lung tumors was observed at a dose of 1% γ-oryzanol, but not at lower doses.

1.7. γ- Oryzanol and non-small cell lung cancer: Hypotheses and objectives

The reported cytotoxic activity of rice bran oil in A549 cells makes it an interesting target in the search for anti-carcinogenic phytochemicals. The evidence that γ-oryzanol, the major component of rice bran oil, has anti-cancer effects on other types of cancer raises the question of whether γ-oryzanol has cytotoxic effects on NSCLC. γ-Oryzanol is not a single compound, but a mixture of steryl ferulates where 24-mCAF, CAF, CMF and β-SF are the most abundant ones, which leads to the question of what are the bioactive compounds in this mixture. The purpose of this study was to answer these questions by analyzing whether 24-mCAF, CAF, CMF and β-SF (γ-oryzanols) have anti-cancer activity against NSCLC and, if so, what are their mechanisms of action.

The first objective of this study was to test the effect of γ-oryzanols on A549 cells viability using a methylthiazol tetrazolium (MTT) assay (Table 2.1). This colorimetric assay uses a tetrazolium dye (3-(4,5-dimethylthiazol-2-yl)-2,5-diphenyltetrazolium bromide) that, when it is reduced by the mitochondrial NAD(P)H oxidoreductases, turns into an insoluble purple formazan. This formazan can be dissolved using dimethyl sulfoxide (DMSO) and the absorbance of the resulting solution reflects the number of viable cells (Mosmann et al., 1983). Cell viability was expected to be affected by some γ-oryzanols, but not necessarily by all of them.

As a second objective, a quantitative proteomics approach was taken to understand the molecular changes caused by γ-oryzanols on A549 cells. Isobaric tags for relative and absolute quantification (iTRAQ) were used to quantify changes in protein expression (Table 2.2). These tags have identical overall mass, but there are 8 versions that vary in terms of the distribution of the heavy carbon and nitrogen isotopes within their structure. They are formed by a peptide reactive group, a balance group and a reporter group (Figure 5). The peptide reactive group labels peptides through free amine groups in the *N*-termini and lysine side chains. When a labeled peptide is fragmented, the reporter ions are released. The intensity of the signals of the reporter ions allows for calculating the relative abundance of peptides (Unwinn et al., 2010). γ-Oryzanols were expected to affect the expression of proteins involved in the regulation of apoptosis and cell cycle progression, as they have shown to do in prostate cancer cells.

In order to validate the results obtained, the third objective of this study was to analyze the expression changes of proteins of interest using a different technique (Table 2.3). Western

blot was chosen as a validation method. Together, these experiments allowed determining the effect of γ-oryzanol on NSCLC at the cellular and molecular level, providing a possible candidate for NSCLC treatment or prevention.

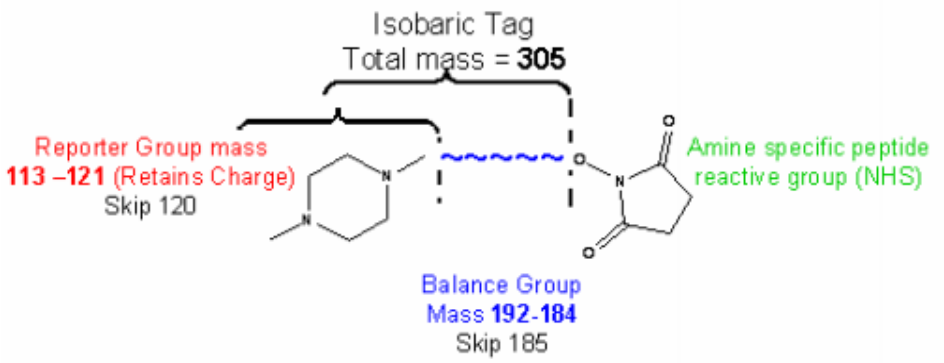

Figure 5. Structure of iTRAQ labels

Table 2. Summary of objectives, methodology and specific hypotheses

2.1 Objective 1	Effect of γ-oryzanols on cell viability of A549 cells	**Hypothesis:** γ-Oryzanols inhibit cell viability of A549 cells. **Methods:** MTT assay
2.2 Objective 2	Quantification of the changes in protein expression in response to γ-oryzanols	**Hypothesis:** γ-Oryzanols affect the expression of proteins involved in apoptosis and cell cycle progression. **Methods:** iTRAQ, SCX, LC-MS/MS, IPA
2.3 Objective 3	Validation of results	**Hypothesis:** Expression changes of proteins of interest are consistent using different methods. **Methods:** Western Blot

CHAPTER 2. METHODOLOGY

2.1. Cell culture

A549 human adenocarcinoma epithelial cells were obtained from the American Type Culture Collection (ATCC). Cells were cultured in Dulbecco's Modified Eagle Medium (DMEM, high glucose, pyruvate) supplemented with 10% v/v fetal bovine serum (FBS), 100 U/mL penicillin and 100µg/mL streptomycin. From now on, this composition will be referred to as "complete DMEM". Cells were grown at 37 ºC and 5% CO_2.

2.2. Cell viability assay

Cells were seeded in 96-well plates at a concentration of 10^4 cells per well in 100 µL of complete DMEM and incubated for 24 hours. They were starved with FBS-free medium for 24 hours. γ-Oryzanols (24-mCAF, CAF, CMF and β-SF) were added in increasing concentrations (10, 25, 50 and 75 µM). DMSO was used as a carrier for γ-oryzanol; the final concentration of DMSO in each condition was 0.75% v/v. There were three biological replicates of each treatment. Cells were treated for 72 hours and they were then incubated with 200 µL of 500 µg/mL MTT for 4 hours. The supernatant was removed, 200 µL of DMSO were added and the optical density was read at 550 nm (OD_{550}).

2.3. Protein extraction

Cells were plated in 75 cm^2 culture flasks in complete DMEM. When they reached approximately 50% confluence, they were starved with 0.05% v/v FBS for 24 hours. Cells were treated with 50 µM 24-mCAF for 72 hours and a control culture was treated with DMSO (the total amount of DMSO in both conditions was 0.5% v/v. Four biological replicates of each condition were used. After 72 hours of treatment, cells were harvested using a cell scraper and washed 3 times with phosphate buffered saline (PBS), centrifuging at 2,000 rpm for 10 minutes each time. Pellets were resuspended in 0.5 mL lysis buffer (10 mM Tris, pH 7.4, 100 mM NaCl, 1 mM EDTA, 2 mM Na_3VO_4, 1 mM EGTA, 1 mM NaF, 20 mM $Na_4P_2O_7$, 1% v/v Triton X-100, 10% v/v glycerol, 0.1% v/v SDS, 0.5% v/v deoxycholate, Halt™ protease inhibitor cocktail) and incubated for 30 minutes, mixing on a vortex every 10 minutes. Lysates were then sonicated in ice using an ultrasonic cell disruptor for 15 seconds, 3 times, waiting 2 minutes in between, and centrifuged for 10 minutes at 13,000 rpm and 4 ºC to. Supernatant was transferred to a clean tube.

Protein concentration was measured according to the Bradford method. Samples were diluted 1:8 and 4 µL were mixed with 200 µL of Biorad Protein Assay Dye diluted 1:5 in a 96-well microtiter plate. Bovine serum albumin (BSA) was used as a calibrator. Absorbance was read at 595 nm.

2.4. Buffer exchange and sample concentration

To avoid the presence of components from the lysis buffer that could interfere with the iTRAQ labeling reaction, buffer was exchanged to 1 M TEAB pH 8.5 using an Amicon Ultra-0.5 mL 3K centrifugal filter. The sample was concentrated to 100 µL.

2.5. Protein digestion

One hundred micrograms of each sample (4 controls and 4 treated) were transferred to new tubes and volume was adjusted to 20 µL with TEAB buffer. Proteins were denatured and reduced using 0.05% v/v SDS and 5 mM tris(2-carboxyethyl)phosphine (TCEP) and incubating at 60 ºC for 1 hour. Cysteine residues were alkylated with 10 mM methylmethanethiosulfate (MMTS) for 10 minutes at room temperature. Proteins were digested by adding 5 µg of sequencing-grade modified porcine trypsin resuspended in water and incubating at 37 ºC for 14 hours.

2.6. iTRAQ labeling

iTRAQ-8plex reagents were resuspended in 50 µL of isopropanol, added to the samples and allowed to react for 2 hours at room temperature. Labels 113, 114, 115 and 119 were used on the control samples; labels 116, 117, 118 and 121 were used on the treated samples. After labeling, samples were pooled together and TEAB buffer was evaporated on a SpeedVac, adding water to avoid dryness. The sample was then resuspended in 100 µL SCX-A (7 mM KH_2PO_4, 30% ACN, pH 2.65) and pH was adjusted to < 2.65 using phosphoric acid.

2.7. Sample fractionation - SCX chromatography

Sample was fractionated using strong cation exchange chromatography (SCX) on an Agilent 1100 high performance liquid chromatography (HPLC) system equipped with a diode array detector and with a polysulfoethyl aspartamide column (2.1 x 200 mm, 5 µm beads, 200 Å pore size). One hundred microliters of sample were injected and the flow rate was 0.2 mL/min. Elution gradient was 5 minutes of 100% SCX-A, 0-30% SCX-B (7 mM KH_2PO_4,

30% ACN, 500 mM KCl, pH 2.65) in 10 min, 30-60% SCX-B in 20 min, 60-100% SCX-B in 5 min, 100% SCX-B for 5 min and 100% SCX-A for 15 min. One-minute fractions were collected from 5 to 60 min after the start of the gradient. Fraction volume was reduced to 100 µL in SpeedVac and fractions were desalted using 100 µL ZipTip C18 tips.

2.8. LC-MS/MS analysis

A nanoAdvance UHPLC coupled to a maXis impact mass spectrometer equipped with a CaptiveSpray source (Bruker) and a Magic C18AQ reversed-phase, 0.1 x 150 mm, 3µm particles and 200 Å pore size analytical column was used. Elution was with a gradient from 5% to 45% solvent B in 80 minutes at a flow rate of 500 nL/min. Solvent A was 0.1% v/v formic acid (FA), 5% v/v acetonitrile (ACN) and 95% v/v LC-MS-grade water. Solvent B was 0.1% v/v FA, 95% v/v ACN and 5% v/v water. Samples were measured in auto MS/MS mode, with a mass range of *m/z* 50-2200. Acquisition speed was 2 Hz in MS and 4 or 16 Hz in MS/MS mode depending on precursor intensity. Precursors were selected in the *m/z* 300-1221 and 1225-2200 range with charge states at 2-5 (singly charge ions were excluded). Active exclusion was activated after 1 spectrum for 2 minutes.

2.9. Data analysis

Peak list files in mascot generic file (mgf) format were generated using DataAnalysis software and submitted to ProteinScape (Bruker). Swissprot was used as a database for Mascot searches. The peptide and MS/MS tolerance were set to 50 ppm and 0.06 Da, respectively. Two missed cleavages were allowed. Methylthio (C) and iTRAQ-8plex (K and N-term) were added as fixed modifications. Oxidation (M) and iTRAQ-8plex (Y) were added as variable modifications. Proteins with a score below 20 and peptides with a score below 15 were discarded.

Quantification ratios were obtained using WARP-LC (Bruker). In order to set up a cutoff ratio that will determine which proteins are up- and down-regulated, and also to identify proteins that were consistently expressed in the control samples, all ratio possibilities between the 4 controls were calculated (114/113, 115/113, 119/113, 115/114, 119/114 and 115/119). Ratios were normalized dividing by the overall median. The logarithm of the median of all control normalized ratios was plotted against the mascot score for each protein (Figure 6). This plot helped to set up a cutoff of 1.25. Proteins inside this range are considered to be consistently expressed in the control samples; proteins outside of this range

are considered to have different expression in the different control samples and were not accepted for further analysis.

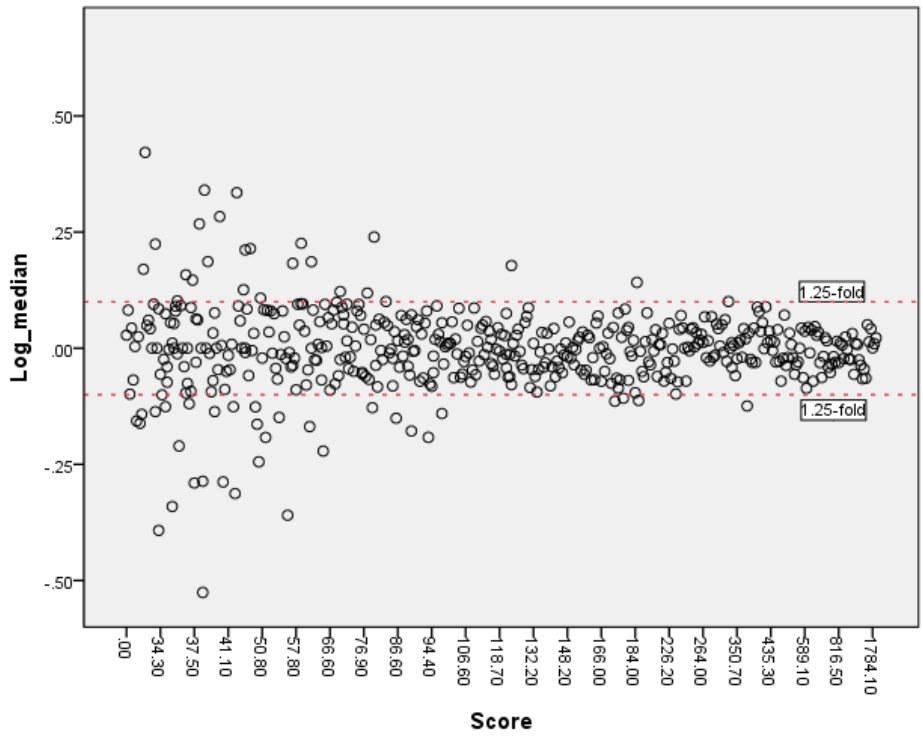

Figure 6. Plot of the logarithm of the median of all possible control/control ratios against the Mascot score. Dashed red lines mark the ± 1.25-fold cutoff. Dots that fall inside the region marked by the lines represent proteins that are considered to be consistently expressed among the control samples and that were accepted for further analysis. Dots that fall outside the lines represent proteins which expression seems not to be consistent among the control samples and were not considered for further analysis.

All combinations of treatment/control ratios were calculated for the accepted proteins (116/113, 117/113, 118/113, 121/113, 116/114, 117/114, 118/114, 121/114, 116/115, 117/115, 118/115, 121/115, 116/119, 117/119, 118/119 and 121/119). Ratios were normalized dividing by the overall median. The median of all normalized ratios was calculated for each protein and the 1.25-fold cutoff was applied to determine what proteins were up- and down-regulated. Results were loaded into IPA for protein function analysis.

2.10. Western blot

Equal amounts of cell lysate (40 µg) were separated by sodium dodecyl sulfate polyacrylamide gel electrophoresis (SDS-PAGE) with an 8% v/v polyacrilamide gel. Proteins were transferred to a polyvinylidene difluoride (PVDF) membrane (0.2 µm pore size) by

elecroblotting for 90 minutes at 100 V using Mini Trans-Blot Electrophoretic Transfer Cell (Bio-Rad). Transfer buffer was 25 mM Tris, 192 mM glycine, 20% v/v ethanol. Membrane was blocked with 3% w/v BSA in Tris-buffered saline, 0.1% v/v Tween 20 (TBST) buffer for 1 hour at room temperature. Primary antibodies were rabbit anti-MYBBP1A and mouse anti-β-actin diluted at 1:1,000 in 1% w/v BSA in TBST. MYBBP1A (148 kDa) was the target protein and β-actin (42 kDa) was used as a loading control. Membrane was cut in half between the 50-75 kDa molecular weight marker bands; the top part was incubated with anti-MYBBP1A primary antibody overnight at 4 ºC, while the bottom part was incubated with anti-β-actin primary antibody. Secondary antibodies were alkaline phosphatase conjugated anti-rabbit/anti-mouse IgG diluted at 1:3,000 in 1% w/v BSA in TBST buffer. Membranes were washed 3 times for 5 minutes with TBST buffer, incubated with corresponding secondary antibody for 1 hour at room temperature and washed again 3 times for 5 minutes with TBST buffer. Alkaline phosphatase conjugate substrate kit (Bio-Rad) was used to measure alkaline phosphatase activity. Membranes were conjugated with substrate for 20 minutes, washed for 10 minutes in deionized water, dried for 5 minutes in an incubator at 30 ºC and scanned. ImajeJ was used to measure band density. The density of the MYBBP1A bands was normalized dividing by the density of the β-actin bands for each sample. Normalized MYBBP1A densities were used to calculate the treated/control expression ratio.

CHAPTER 3. RESULTS

3. 1. Effect of γ-oryzanols on cell viability of A549 cells

Cytotoxicity of the major components in γ-oryzanol (24-mCAF, CAF, CMF and β-SF) on A549 NSCLC cells was tested using an MTT assay. Figure 1 shows the results, where cell viability is represented as a percentage of the control. 24-mCAF, CAF and CMF showed significant inhibition of cell viability, whereas β-SF did not seem to affect it. Among the four γ-oryzanols, 24-mCAF showed the strongest inhibition, which was significant from a concentration of 10 µM. Given these results, 24- mCAF was selected for further study. A concentration of 50 µM was chosen to ensure an inhibition of more than 40%.

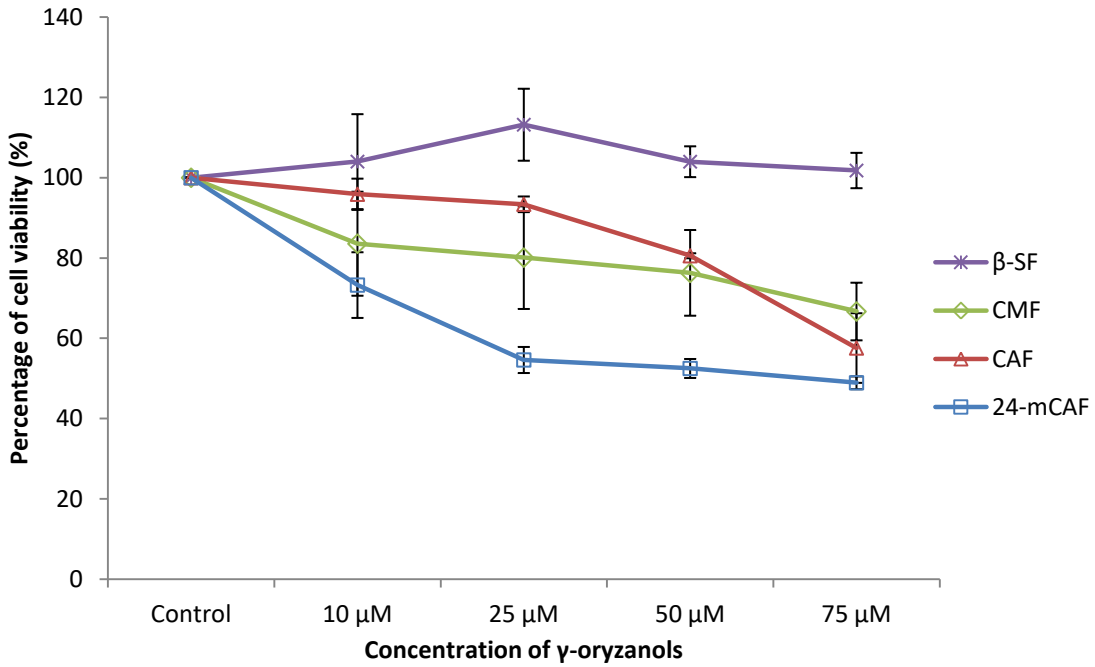

Figure 7. Effect of γ-oryzanols on cell viability of A549 cells. Cell viability is represented as a percentage of the control. Error bars represent the standard deviation of the mean (SEM). Sample size (n) = 3

3. 1. Quantitative analysis of the changes in protein expression in response to 24-mCAF

In order to analyze the effect of 24-mCAF in protein expression, an iTRAQ-based quantitative proteomic analysis was carried out. A total of 484 proteins were identified. However, only 432 were considered to be consistently expressed in the control samples and were accepted for analysis (see Section 2.9). A 1.25-fold cutoff was used to determine which

proteins were differentially expressed. Distribution of the ratios can be observed in Figure 8, where the logarithm of the median is represented against the Mascot score for each protein. A total of 58 differentially expressed proteins were identified, 29 of which were up-regulated and 29 down-regulated (Appendix).

Differentially expressed proteins were subjected to IPA and the results revealed that 32 of them were cytoplasmic proteins, 18 nuclear, 6 from the plasma membrane and 2 extracellular. Twenty of these proteins were enzymes, 9 were transcription factors and 5 were transporters (Figure 9). Cellular functions analysis indicated that cell death, apoptosis and cell proliferation were the most affected cellular processes by 24-mCAF (Table 3). Cell death and apoptosis where activated, whereas cell proliferation was inactivated. Eighteen of the differentially expressed proteins contributed to the activation of cell death, 14 to the activation of apoptosis and 11 to the inactivation of cell proliferation.

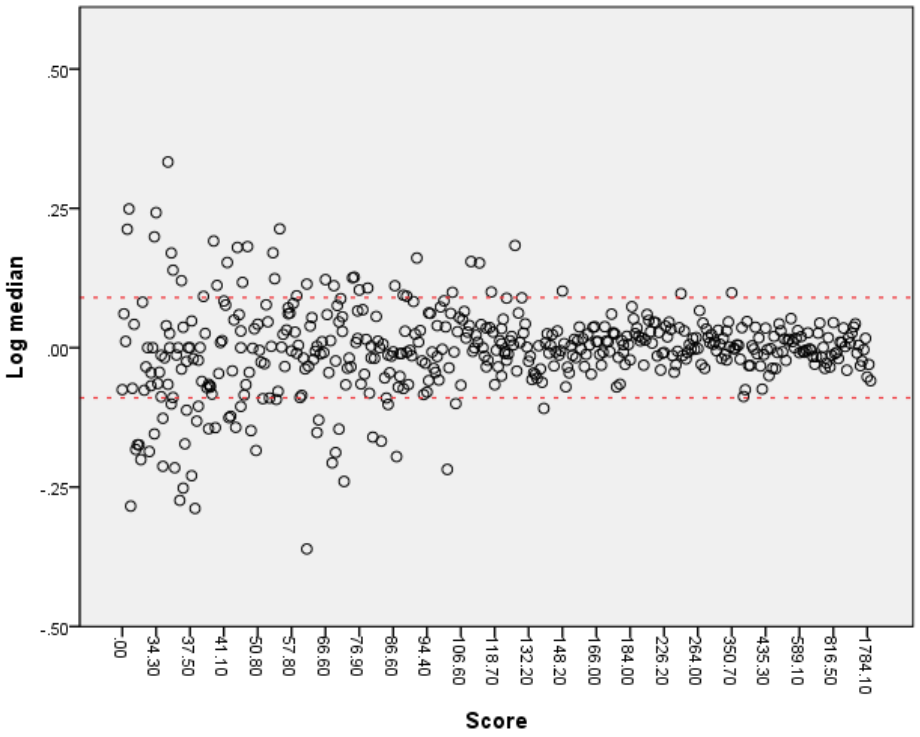

Figure 8. Plot of the logarithm of the median of all possible treated/control ratios against Mascot score. Dashed red lines indicate the ±1.25-fold cutoff. Dots outside this range represent proteins that are considered to be up- or down-regulated by 24-mCAF

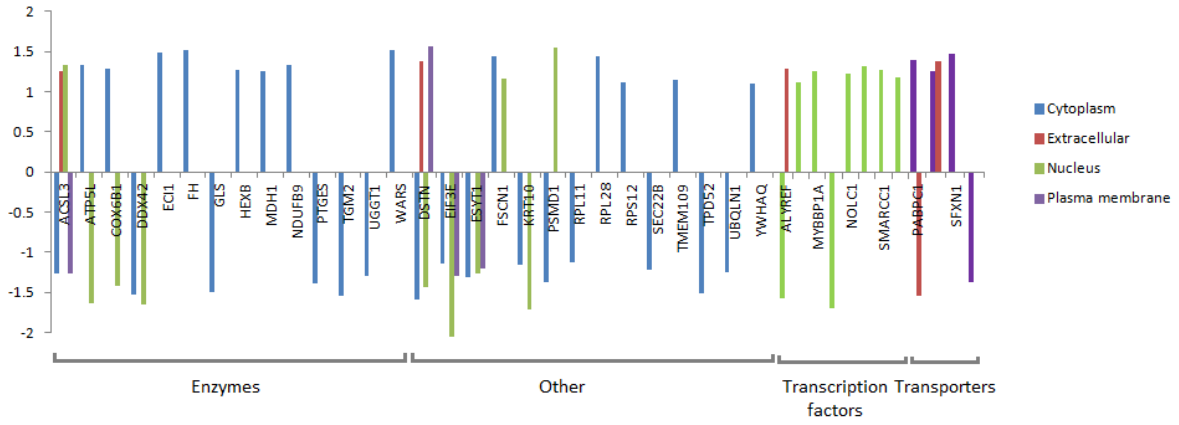

Figure 9. Differentially expressed proteins after treatment with 24-mCAF. Y-axis represents the median of all possible treated/control ratios. X-axis shows the protein ID. Color code indicates in which cell compartment proteins are present. Grey labels at the bottom classify proteins by their function.

Table 3. Most affected cellular functions by 24-mCAF.

Cellular functions	Activation State	P-value overlap	z-score		Contributing proteins
Cell death	Activated	1.67E-07	1.477	18	↑SMARCC1, ↓TPD52, ↓TOP2B, ↓TGM2, ↓UBQLN1, ↑MYBBP1A, ↓GLS, ↓SNRPB, ↓NAA15, ↓PSMC6, ↓ATP1A2, ↓ITGA3, ↓SF3B1, ↓SLC25A10, ↓VAPB, ↓EIF3E, ↓RPL11, ↑FH
Apoptosis	Activated	9.32E-05	2.062	14	↑SMARCC1, ↓TPD52, ↓TOP2B, ↓UBQLN1, ↓SLC25A10, ↓ITGA3, ↑MYBBP1A, ↓GLS, ↓SF3B1, ↓ATP1A2, ↑FH, ↓NAA15, ↑TMEM109, ↑HEXB
Cell proliferation	Inactivated	1.27E02	-0.908	11	↑WARS, ↓TPD52, ↓TGM2, ↓SF3B1, ↑SEC23A, ↓PTGES, ↓ITGA3, ↑GPI, ↓GLS, ↓EIF3E, ↓CA12

Myb binding protein 1A (MYBBP1A) is a transcriptional regulator that acts as tumor suppressor by binding to several proteins involved in cancer progression. These proteins include P53, NFκB and sirtuin 6 (SIRT6). In this study, MYBBP1A was found to be up-regulated by 24-mCAF. P53 is a transcription factor well known for its role in cell cycle control; its interaction with MYBBP1A allows its activation and induces cell cycle arrest and apoptosis. NFκB controls inflammatory processes and cell survival; MYBBP1A inhibits transcription of NFκB, leading to inhibition of these processes. SIRT6 is a deacylase known

to act as a metastasis-inducing protein in NSCLC. It inactivates a series of transcription factors that control the expression of a large amount of proteins, including the tumor protein D52 (TPD52), NADH dehydrogenase ubiquinone 1 beta subcomplex subunit 9 (NDUFB9), enoyl-CoA delta isomerase 1 (ECI1), fumarate hydratase (FH), malate dehydrogenase (MDH1), vesicle-trafficking protein SEC22B, SEC23A and UPD-glucose glycoprotein glucosyltransferase 1 (UGGT1). These 8 proteins were found to be differentially expressed after treatment with 24-mCAF and their up- or down-regulation is consistent with inactivation of SIRT6. TPD52 and SEC22B are typically over-expressed in NSCLC; they act inducing cell migration and invasion and they were down-regulated by 24-mCAF. NDUFB9, FH and SEC23A are tumor suppressive proteins involved in the control of cell invasion which down-regulation is associated with metastasis. These proteins were up-regulated by 24-mCAF. The results suggest that the up-regulation of MYBBP1A contributes to stop cancer progression via its interaction with proteins directly involved in cancer related processes, such as P53 and NFκB, and through the inactivation of SIRT6, which leads to the up- or down- regulation of TPD52, NDUFB9, ECI1, FH, MDH1, SEC22B, SEC23A and UGGT1 (Figure 10).

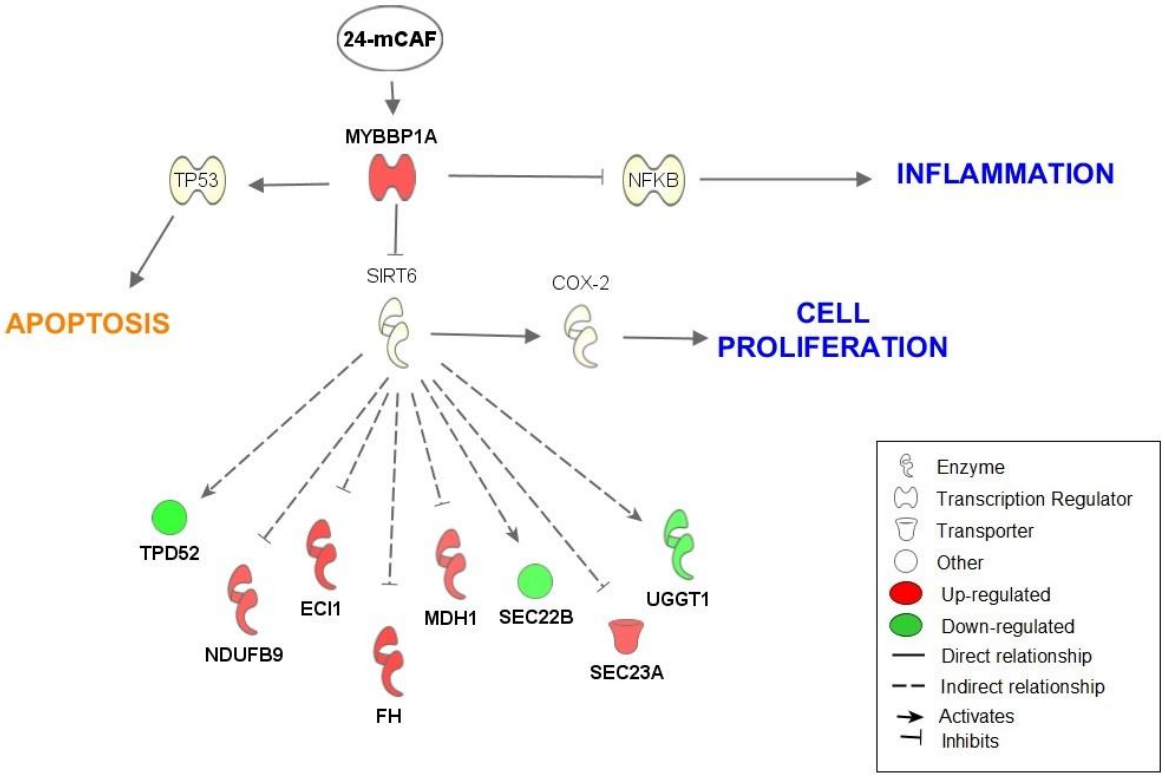

Figure 10. Proposed mechanism of action of 24-mCAF in A549 cells

3. 3. Western Blot

Although 24-mCAF is likely to stop cancer progression through different mechanisms, the one proposed above connects the higher number of differentially expressed proteins detected in this study. Therefore, up-regulation of MYBBP1A was verified by western blot. Band density for MYBBP1A was normalized with band density for β- actin. Results are shown in Figure 11. MYBBP1A was significantly over-expressed in the sample treated with 24-mCAF compared to the control sample. These results confirm the ones obtained with iTRAQ.

(A)

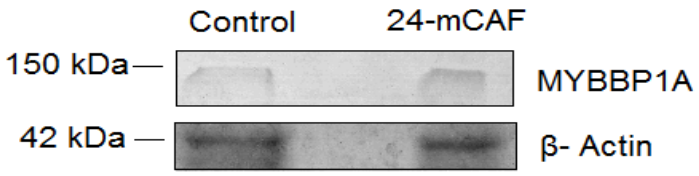

(B)

Protein	iTRAQ ratio	Western blot ratio
MYBBP1A	1.42	1.50

Figure 11. Western blot analysis of the differential expression of MYBBP1A in A549 cells treated and non-treated with 24-mCAF.

CHAPTER 4. DISCUSSION

NSCLC is the most common type of cancer. Its increasing prevalence and the lack of effective treatments make the need to find new alternatives to prevent or treat this disease a matter of great importance. γ-Oryzanol is a mixture of steryl ferulates found in rice and other cereal grains that has shown to have numerous health benefits, including anti-cancer activity in prostate cancer cell lines. The goal of this study was to determine whether the most abundant components in the γ-oryzanol mixture (24-mCAF, CAF, CMF and β-SF) have cytotoxic activity against A549 NSCLC cells and what are the molecular changes that lead to this effect.

First, the effect of 24-mCAF, CAF, CMF and β-SF on cell viability of A549 cells was tested. Results showed that 24-mCAF, CAF and CMF significantly inhibited cell proliferation, whereas β-SF did not seem to affect it (Figure 6). From all compounds, 24-mCAF was the one that showed the highest inhibitory effect, which was significant from a concentration of 10 µM after 72 hours of treatment. This concentration is around 100 times lower than the concentrations reported for prostate cancer cell lines by Klongpityapoing et al. (2013). This might be due to the fact that in previous studies the cytotoxicity of γ-oryzanol on cancer cells was tested applying γ-oryzanol as a mixture. Here, the most abundant components of γ-oryzanol were individually tested and not all of them showed cytotoxicity. This would explain that the whole mixture has a weaker effect than the pure compounds. Therefore, 24-mCAF was selected as the treatment for further experiments.

In order to better understand the effect of γ-oryzanol on NSCLC, the changes that it causes in the proteome were analyzed. A quantitative proteomic approach based on iTRAQ was used to identify proteins that were differentially expressed after treatment with 50 µM 24-mCAF for 72 hours. Although the effects on cell viability of this compound were significant from 10 µM, a higher concentration was chosen to ensure that there were detectable changes in protein expression. A total of 58 differentially expressed proteins were identified, 29 of which were up-regulated and 29 down-regulated (Figure 9).

Analysis with IPA revealed that the cellular processes that were most affected by 24-mCAF were cell death, apoptosis, and cell proliferation (Table 3). Cell death and apoptosis were activated, whereas cell proliferation was inhibited. There were 18 differentially expressed proteins contributing to the activation of cell death, 14 to the activation of apoptosis and 11 to

the inhibition of cell proliferation. These results are consistent with the cell viability experiments and show that γ-oryzanol has cytotoxic activity on A549 cells. These findings also correlate with previous studies in prostate cancer cells, where γ-oryzanol showed to induce apoptosis and block cell cycle progression (Hirsch et al., 2015).

MYBBP1A is a transcriptional regulator localized in the nucleolus that plays an important role in early embryonic development and the regulation of inflammation and cell cycle progression (George et al., 2015). MYBBP1A acts as a tumor suppressor and it is up-regulated by 24-mCAF. It was first known to be a c-Myb interacting protein, but it was later reported to bind a number of different transcription factors, including P53 and NFκB. (Perrera et al., 2010). When nucleolar disruption occurs, MYBBP1A is translocated to the nucleoplasm, where it binds P53 and facilitates its tetramerization and activation, inducing cell cycle arrest and apoptosis (Ono et al., 2014). MYBBP1A is also a repressor of NFκB, which leads to inhibition of inflammatory processes (Owen et al., 2007). Inhibition of NFκB by γ-oryzanol was previously reported by Sakai et al. (2012).

MYBBP1A is also known to bind SRIT6, a member of the mammalian sirtuin family (Polyakova et al., 2012). Sirtuins are a conserved group of NAD^+ dependent proteins with deacylase and/ or ADP ribosyltransferase activitiy. SIRT6 possess both activities and acts as a regulator of several processes, such as DNA repair, gene expression, telomere maintenance, metabolism and aging. This protein plays multiple complex roles in cancer; depending on the type of cancer, it can act as a tumor suppressor or as a cancer-inducing protein. In NSCLC, SIRT6 is up-regulated. Knockdown of SIRT6 in A459 cells reduces cell migration and invasion, whereas its over-expression induces metastasis (Bai et al. 2016). SIRT6 promotes the expression of COX-2, a tumor-inducing protein that is involved in cell proliferation and survival (Ming et al., 2014). Up-regulation of MYBBP1A produces inactivation of SIRT6, which leads to down-regulation of COX-2 and consequently to the inhibition of cell proliferation. Reduction of the expression of COX-2 by γ-oryzanol was previously reported by Szcześniak et al. (2015).

SIRT6 is known to indirectly regulate the expression of numerous proteins, including TPD52, NDUFB9, ECI1, FH, MDH1, SEC22B, SEC23A and UGGT1. These 8 proteins were found to be differentially expressed in this study, and their expression direction indicates that SITR6 is inactivated. TPD52, SEC22B and UGGT1 were down-regulated by 24-mCAF, whereas

NDUFB9, ECI1, FH, MDH1 and SEC23A were up-regulated. The differential expression of most of these proteins is consistent with cancer inhibition.

TPD52 is over-expressed in lung adenocarcioma; its gene is located in chromosome 8q21.13, which is one of the most amplified genomic regions in this type of cancer. Its over-expression enhances cancer cell aggressiveness and contributes to several oncogenic pathways. Knockdown of TPD52 significantly suppresses cancer cell migration and invasion (Kumamoto et al., 2016).

SEC22B is a vesicle-trafficking protein that is involved in lipid metabolism at contact sites between the endoplasmic reticulum (ER) and the plasma membrane. Lipid production and transfer at these membrane contact sites are essential for membrane expansion, which is important in cell migration (Petkovic et al., 2014). Okayama et al. (2014) carried out a proteomic study to identify proteins related to prognosis in lung adenocarcinoma and found that SEC22B was over-expressed in patients with poor prognosis.

NDUFB9 is an accessory subunit of the mitochondrial membrane respiratory chain NADH dehydrogenase (Complex I) and it is down-regulated in highly metastatic cancer cells. Down-regulation of NDUFB9 produces complex I deficiency, which disturbs electron transfer and leads to a disruption of the NAD^+/NADH balance. Together with other processes, this unbalance induces cell migration and invasion (Li et al. 2015).

FH converts fumarate to malate in the tricarboxylic acid cycle. Its down-regulation increases the amount of intracellular fumaric acid, which inhibits the hydroxylation of the hypoxia-inducible factor (HIF). If HIF cannot be hydroxylated, it cannot be degraded by the proteosome. HIF regulates the expression of several genes like vascular endothelial growth factor (VEGF), erythropoietin (EPO), platelet derived growth factor (PDGF), EGFR, glucose transporter protein 1 (GLUT-1), and transforming growth factor-alpha (TGF-α). These genes are involved in maintaining the energy metabolism of tumor cells, promoting tumor angiogenesis, invasion, and metastasis. In A549 cells, FH is significantly under-expressed at both mRNA and protein levels compared with non-cancer cells (Ming et al., 2014).

MDH1 catalyzes the conversion of malate to oxaloacetate in the cytoplasm and it has also been reported to be a transcriptional co-activator of P53. It stabilizes and activates it by translocating to the nucleus and binding to p53-responsive elements in the promoter of downstream genes. When MDH1 is down-regulated, binding of acetylated P53 is

significantly reduced, which results in loss of p53-mediated cell cycle arrest and apoptosis (Lee et al., 2009).

SEC23A is an indispensable component of coat protein Complex II (COPII)-coated vesicles that is involved in transporting secretory proteins from the ER to the Golgi apparatus. SEC23A is essential for the secretion of components of the extracellular membrane, such as collagen and cartilage oligomeric matrix protein, and it is also important in the secretion of metastasis suppressive proteins, like Igfbp4 and Tinagl1 (Boyadjiev et al., 2006). Korpal et al. (2012) reported that knockdown of SEC23A enhanced metastatic colonization; however, overexpression of SEC23A alone was not sufficient to significantly suppress metastasis.

Given the results obtained, 24-mCAF seems to inhibit cancer progression by causing MYBBP1A up-regulation, which contributes to stop cancer progression through different mechanisms (Figure 12). Up-regulation of MYBBP1A by 24-mCAF was verified with western blot and the results were consistent with those obtained with iTRAQ (Figure 11). Nevertheless, this proposed mechanism does not explain all the expression changes detected in this study, indicating that 24-mCAF is likely to stop cancer progression via different mechanisms.

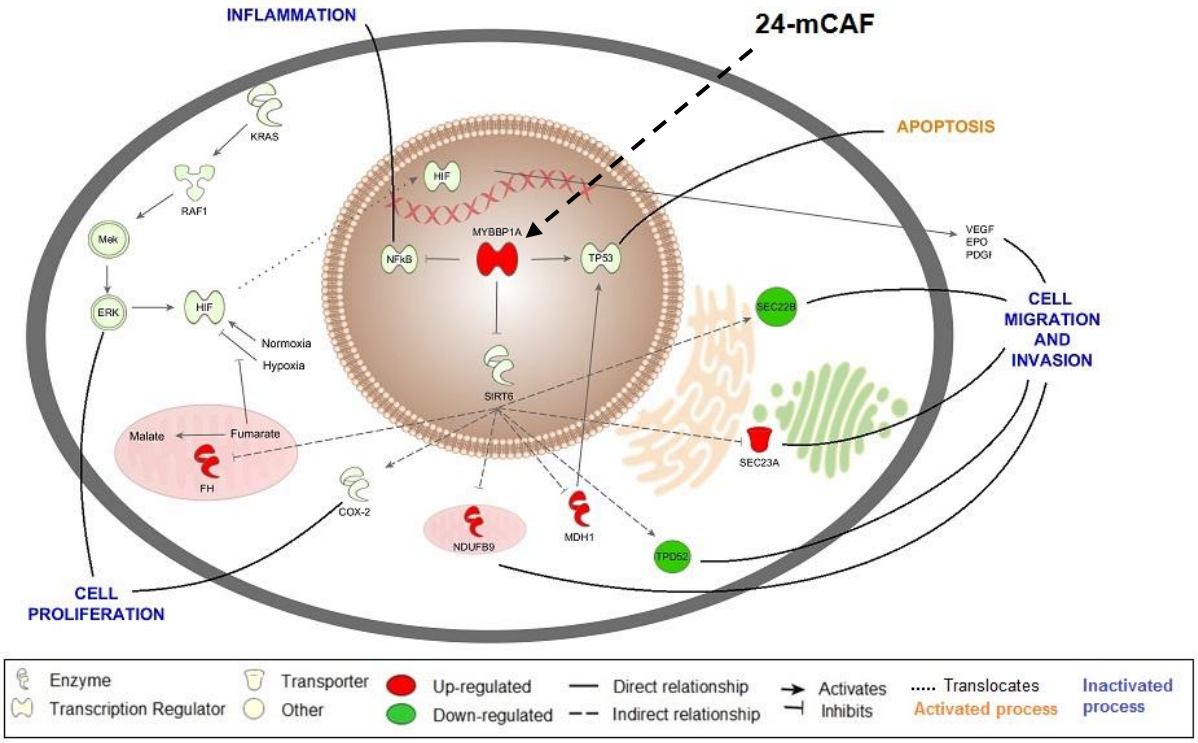

Figure 12. Cellular diagram of the proposed mechanism of action of 24-mCAF in A549 cells

CHAPTER 5. SUMMARY

The results obtained in this study show that 24-mCAF inhibits cell proliferation of A549 cells. Anti-cancer effects of γ-oryzanol as a mixture have previously been reported for other types of cancer, but not for NSCLC. Here, the 4 most abundant components of γ-oryzanol (24-mCAF, CAF, CMF and β-SF) were individually tested. 24-mCAF, CAF and CMF inhibited cell proliferation, while β-SF did not. 24-mCAF showed the strongest inhibitory effect.

A quantitative proteomic study using iTRAQ confirmed the cytotoxic effect of 24-mCAF on A549 cells. The most affected molecular functions by the changes caused in the proteome were cell death and apoptosis, which were activated, and cell proliferation, which was inactivated. The results obtained suggest that 24-mCAF produces MYBBP1A up-regulation, which leads to cancer inhibition through different mechanisms. These mechanisms include its interaction with P53, which induces apoptosis and cell cycle arrest; its interaction with NFκB, which inhibits inflammatory processes; and its interaction with SIRT6, which leads to the down-regulation of TPD52, SEC22B and UGGT1 and to the up-regulation of NDUFB9, ECI1, FH, MDH1 and SEC23A. However, this proposed mechanism does not explain the up- or down-regulation of all differentially expressed proteins detected, which suggests that 24-mCAF probably affects the cell in different ways and inhibits cancer through different mechanisms.

CHAPTER 6. APPENDIX

Accession[1]	Protein	MW[2] [kDa]	Scores[3]	#Peptides[4]	SC[5] [%]	iTRAQ[6] ratio
CD59_HUMAN	CD59 glycoprotein OS=Homo sapiens GN=CD59 PE=1 SV=1	14.2	25.9	1	9.4	1.77
NH2L1_HUMAN	NHP2-like protein 1 OS=Homo sapiens GN=SNU13 PE=1 SV=3	14.2	34.3	1	9.4	1.75
FSCN1_HUMAN	Fascin OS=Homo sapiens GN=FSCN1 PE=1 SV=3	54.5	55.6	2	7.5	1.63
RL28_HUMAN	60S ribosomal protein L28 OS=Homo sapiens GN=RPL28 PE=1 SV=3	15.7	22.8	1	5.1	1.63
NENF_HUMAN	Neudesin OS=Homo sapiens GN=NENF PE=1 SV=1	18.8	39.9	1	5.2	1.55
SFXN1_HUMAN	Sideroflexin-1 OS=Homo sapiens GN=SFXN1 PE=1 SV=4	35.6	128.1	3	9.9	1.53
SYWC_HUMAN	Tryptophan--tRNA ligase, cytoplasmic OS=Homo sapiens GN=WARS PE=1 SV=2	53.1	48.5	1	3.4	1.52
FUMH_HUMAN	Fumarate hydratase, mitochondrial OS=Homo sapiens GN=FH PE=1 SV=3	54.6	43.2	1	3.5	1.51
SMAD9_HUMAN	Mothers against decapentaplegic homolog 9 OS=Homo sapiens GN=SMAD9 PE=1 SV=1	52.5	53.8	1	2.8	1.48
ECI1_HUMAN	Enoyl-CoA delta isomerase 1, mitochondrial OS=Homo sapiens GN=ECI1 PE=1 SV=1	32.8	36	1	4.3	1.48
PABP1_HUMAN	Polyadenylate-binding protein 1 OS=Homo sapiens GN=PABPC1 PE=1 SV=2	70.6	93.2	3	5.7	1.45
LAT1_HUMAN	Large neutral amino acids transporter small subunit 1 OS=Homo sapiens GN=SLC7A5 PE=1 SV=2	55	110.7	3	5.3	1.43
SMRC1_HUMAN	SWI/SNF complex subunit SMARCC1 OS=Homo sapiens GN=SMARCC1 PE=1 SV=3	122.8	41.5	1	1	1.42
MBB1A_HUMAN	Myb-binding protein 1A OS=Homo sapiens GN=MYBBP1A PE=1 SV=2	148.8	113	3	2.8	1.42
NOLC1_HUMAN	Nucleolar and coiled-body phosphoprotein 1 OS=Homo sapiens GN=NOLC1 PE=1 SV=2	73.6	36.1	1	2.1	1.38
ATP5L_HUMAN	ATP synthase subunit g, mitochondrial OS=Homo sapiens GN=ATP5L PE=1 SV=3	11.4	74.7	2	27.2	1.34
RAN_HUMAN	GTP-binding nuclear protein Ran OS=Homo sapiens GN=RAN PE=1 SV=3	24.4	74.4	2	11.1	1.33
NDUB9_HUMAN	NADH dehydrogenase [ubiquinone] 1 beta subcomplex subunit 9 OS=Homo sapiens GN=NDUFB9 PE=1 SV=3	21.8	55.3	2	20.1	1.33
ZN207_HUMAN	BUB3-interacting and GLEBS motif-containing protein ZNF207 OS=Homo sapiens GN=ZNF207 PE=1 SV=1	50.7	66.6	1	2.7	1.32
SNRPA_HUMAN	U1 small nuclear ribonucleoprotein A OS=Homo sapiens GN=SNRPA PE=1 SV=3	31.3	44.6	1	6.4	1.31
TM109_HUMAN	Transmembrane protein 109 OS=Homo sapiens GN=TMEM109 PE=1 SV=1	26.2	40.1	1	5.3	1.29
SC23A_HUMAN	Protein transport protein Sec23A OS=Homo sapiens GN=SEC23A PE=1 SV=2	86.1	88	2	4.1	1.29
CX6B1_HUMAN	Cytochrome c oxidase subunit 6B1 OS=Homo sapiens GN=COX6B1 PE=1 SV=2	10.2	68.4	2	20.9	1.29
HEXB_HUMAN	Beta-hexosaminidase subunit beta	63.1	76.9	3	6.1	1.27

	OS=Homo sapiens GN=HEXB PE=1 SV=3					
RS12_HUMAN	40S ribosomal protein S12 OS=Homo sapiens GN=RPS12 PE=1 SV=3	14.5	148.2	4	31.8	1.26
FUBP1_HUMAN	Far upstream element-binding protein 1 OS=Homo sapiens GN=FUBP1 PE=1 SV=3	67.5	117.9	5	7.9	1.26
MDHC_HUMAN	Malate dehydrogenase, cytoplasmic OS=Homo sapiens GN=MDH1 PE=1 SV=4	36.4	103.1	3	11.4	1.26
G6PI_HUMAN	Glucose-6-phosphate isomerase OS=Homo sapiens GN=GPI PE=1 SV=4	63.1	350.7	12	20.6	1.25
1433T_HUMAN	14-3-3 protein theta OS=Homo sapiens GN=YWHAQ PE=1 SV=1	27.7	238.2	6	30.2	1.25
TOM6_HUMAN	Mitochondrial import receptor subunit TOM6 homolog OS=Homo sapiens GN=TOMM6 PE=1 SV=1	8	90	3	41.9	1.24
TMED4_HUMAN	Transmembrane emp24 domain-containing protein 4 OS=Homo sapiens GN=TMED4 PE=1 SV=1	25.9	59	2	7.5	1.24
HYOU1_HUMAN	Hypoxia up-regulated protein 1 OS=Homo sapiens GN=HYOU1 PE=1 SV=1	111.3	128.6	5	8.5	1.23
PARP1_HUMAN	Poly [ADP-ribose] polymerase 1 OS=Homo sapiens GN=PARP1 PE=1 SV=4	113	124.1	4	5.4	1.23
RL9_HUMAN	60S ribosomal protein L9 OS=Homo sapiens GN=RPL9 PE=1 SV=1	21.8	70.2	2	19.3	1.22
KAD2_HUMAN	Adenylate kinase 2, mitochondrial OS=Homo sapiens GN=AK2 PE=1 SV=2	26.5	100.5	3	16.7	1.21
AHSA1_HUMAN	Activator of 90 kDa heat shock protein ATPase homolog 1 OS=Homo sapiens GN=AHSA1 PE=1 SV=1	38.3	41.1	1	6.5	1.21
NP1L1_HUMAN	Nucleosome assembly protein 1-like 1 OS=Homo sapiens GN=NAP1L1 PE=1 SV=1	45.3	91.7	3	12	1.21
CPNE3_HUMAN	Copine-3 OS=Homo sapiens GN=CPNE3 PE=1 SV=1	60.1	32.4	1	1.7	1.21
ACOT1_HUMAN	Acyl-coenzyme A thioesterase 1 OS=Homo sapiens GN=ACOT1 PE=1 SV=1	46.2	58.7	2	6.4	1.20
AN32B_HUMAN	Acidic leucine-rich nuclear phosphoprotein 32 family member B OS=Homo sapiens GN=ANP32B PE=1 SV=1	28.8	53.1	2	10.8	1.19
RT21_HUMAN	28S ribosomal protein S21, mitochondrial OS=Homo sapiens GN=MRPS21 PE=1 SV=2	10.7	41.2	1	13.8	1.19
NDUA5_HUMAN	NADH dehydrogenase [ubiquinone] 1 alpha subcomplex subunit 5 OS=Homo sapiens GN=NDUFA5 PE=1 SV=3	13.5	69.4	2	30.2	1.19
PRS6B_HUMAN	26S protease regulatory subunit 6B OS=Homo sapiens GN=PSMC4 PE=1 SV=2	47.3	99.7	3	10.5	1.18
RS21_HUMAN	40S ribosomal protein S21 OS=Homo sapiens GN=RPS21 PE=1 SV=1	9.1	57.3	2	22.9	1.18
AT2A2_HUMAN	Sarcoplasmic/endoplasmic reticulum calcium ATPase 2 OS=Homo sapiens GN=ATP2A2 PE=1 SV=1	114.7	269.8	9	13.7	1.17
VINC_HUMAN	Vinculin OS=Homo sapiens GN=VCL PE=1 SV=4	123.7	76.3	2	2.8	1.16
BASP1_HUMAN	Brain acid soluble protein 1 OS=Homo sapiens GN=BASP1 PE=1 SV=2	22.7	107.8	3	18.1	1.16
MGST1_HUMAN	Microsomal glutathione S-transferase 1 OS=Homo sapiens GN=MGST1 PE=1 SV=1	17.6	94.8	2	16.1	1.15
SET_HUMAN	Protein SET OS=Homo sapiens GN=SET PE=1 SV=3	33.5	57.5	2	8.3	1.15

LASP1_HUMAN	LIM and SH3 domain protein 1 OS=Homo sapiens GN=LASP1 PE=1 SV=2	29.7	128.3	5	16.1	1.15
HMOX1_HUMAN	Heme oxygenase 1 OS=Homo sapiens GN=HMOX1 PE=1 SV=1	32.8	95.2	3	18.4	1.15
DLDH_HUMAN	Dihydrolipoyl dehydrogenase, mitochondrial OS=Homo sapiens GN=DLD PE=1 SV=2	54.1	102.9	3	11.4	1.15
KLK10_HUMAN	Kallikrein-10 OS=Homo sapiens GN=KLK10 PE=1 SV=3	30.2	15.6	1	2.5	1.15
TCPD_HUMAN	T-complex protein 1 subunit delta OS=Homo sapiens GN=CCT4 PE=1 SV=4	57.9	175	7	21.5	1.15
RS13_HUMAN	40S ribosomal protein S13 OS=Homo sapiens GN=RPS13 PE=1 SV=2	17.2	203.8	6	37.1	1.15
SF3B3_HUMAN	Splicing factor 3B subunit 3 OS=Homo sapiens GN=SF3B3 PE=1 SV=4	135.5	66.9	2	2.7	1.15
IF2B1_HUMAN	Insulin-like growth factor 2 mRNA-binding protein 1 OS=Homo sapiens GN=IGF2BP1 PE=1 SV=2	63.4	82.1	2	5.4	1.14
SODC_HUMAN	Superoxide dismutase [Cu-Zn] OS=Homo sapiens GN=SOD1 PE=1 SV=2	15.9	71.7	2	15.6	1.14
SYRC_HUMAN	Arginine--tRNA ligase, cytoplasmic OS=Homo sapiens GN=RARS PE=1 SV=2	75.3	106.4	4	7.7	1.13
PSB7_HUMAN	Proteasome subunit beta type-7 OS=Homo sapiens GN=PSMB7 PE=1 SV=1	29.9	63	2	6.9	1.13
HNRPM_HUMAN	Heterogeneous nuclear ribonucleoprotein M OS=Homo sapiens GN=HNRNPM PE=1 SV=3	77.5	538.1	18	22.6	1.13
TEBP_HUMAN	Prostaglandin E synthase 3 OS=Homo sapiens GN=PTGES3 PE=1 SV=1	18.7	122.8	4	30.6	1.13
EF1B_HUMAN	Elongation factor 1-beta OS=Homo sapiens GN=EEF1B2 PE=1 SV=3	24.7	107	3	26.7	1.12
EMC7_HUMAN	ER membrane protein complex subunit 7 OS=Homo sapiens GN=EMC7 PE=1 SV=1	26.5	43	1	5.4	1.12
PRDX5_HUMAN	Peroxiredoxin-5, mitochondrial OS=Homo sapiens GN=PRDX5 PE=1 SV=4	22.1	204	6	39.3	1.12
TM9S2_HUMAN	Transmembrane 9 superfamily member 2 OS=Homo sapiens GN=TM9SF2 PE=1 SV=1	75.7	37.7	1	2.1	1.12
EF2_HUMAN	Elongation factor 2 OS=Homo sapiens GN=EEF2 PE=1 SV=4	95.3	394.7	10	15.4	1.11
PSME3_HUMAN	Proteasome activator complex subunit 3 OS=Homo sapiens GN=PSME3 PE=1 SV=1	29.5	69.6	2	8.7	1.11
AL3A2_HUMAN	Fatty aldehyde dehydrogenase OS=Homo sapiens GN=ALDH3A2 PE=1 SV=1	54.8	53.3	2	6	1.11
PDIA4_HUMAN	Protein disulfide-isomerase A4 OS=Homo sapiens GN=PDIA4 PE=1 SV=2	72.9	345	10	18	1.11
NDKB_HUMAN	Nucleoside diphosphate kinase B OS=Homo sapiens GN=NME2 PE=1 SV=1	17.3	233.7	7	43.4	1.11
H2AY_HUMAN	Core histone macro-H2A.1 OS=Homo sapiens GN=H2AFY PE=1 SV=4	39.6	208.7	5	18	1.11
NQO1_HUMAN	NAD(P)H dehydrogenase [quinone] 1 OS=Homo sapiens GN=NQO1 PE=1 SV=1	30.8	217.6	8	20.8	1.11
HS90A_HUMAN	Heat shock protein HSP 90-alpha OS=Homo sapiens GN=HSP90AA1 PE=1 SV=5	84.6	816.5	21	36.1	1.11
ENPL_HUMAN	Endoplasmin OS=Homo sapiens GN=HSP90B1 PE=1 SV=1	92.4	726.9	23	35.7	1.11
ILF3_HUMAN	Interleukin enhancer-binding factor 3 OS=Homo sapiens GN=ILF3 PE=1 SV=3	95.3	275.8	9	12.4	1.11
THIL_HUMAN	Acetyl-CoA acetyltransferase, mitochondrial OS=Homo sapiens GN=ACAT1 PE=1 SV=1	45.2	131.5	6	19.7	1.10

TBB5_HUMAN	Tubulin beta chain OS=Homo sapiens GN=TUBB PE=1 SV=2	49.6	1135.9	29	59	1.10
PDIA3_HUMAN	Protein disulfide-isomerase A3 OS=Homo sapiens GN=PDIA3 PE=1 SV=4	56.7	473.9	17	34.7	1.10
PDCD6_HUMAN	Programmed cell death protein 6 OS=Homo sapiens GN=PDCD6 PE=1 SV=1	21.9	50.8	2	19.9	1.10
RALY_HUMAN	RNA-binding protein Raly OS=Homo sapiens GN=RALY PE=1 SV=1	32.4	29.4	1	2.6	1.10
TCPQ_HUMAN	T-complex protein 1 subunit theta OS=Homo sapiens GN=CCT8 PE=1 SV=4	59.6	113.4	5	12.2	1.10
TXND5_HUMAN	Thioredoxin domain-containing protein 5 OS=Homo sapiens GN=TXNDC5 PE=1 SV=2	47.6	110.5	3	10.6	1.10
CPSM_HUMAN	Carbamoyl-phosphate synthase [ammonia], mitochondrial OS=Homo sapiens GN=CPS1 PE=1 SV=2	164.8	98.4	3	2.5	1.10
2AAA_HUMAN	Serine/threonine-protein phosphatase 2A 65 kDa regulatory subunit A alpha isoform OS=Homo sapiens GN=PPP2R1A PE=1 SV=4	65.3	35.7	1	2.2	1.10
RL24_HUMAN	60S ribosomal protein L24 OS=Homo sapiens GN=RPL24 PE=1 SV=1	17.8	62.2	2	14	1.09
AK1BF_HUMAN	Aldo-keto reductase family 1 member B15 OS=Homo sapiens GN=AKR1B15 PE=1 SV=2	36.5	228.8	4	12	1.09
RL12_HUMAN	60S ribosomal protein L12 OS=Homo sapiens GN=RPL12 PE=1 SV=1	17.8	172	4	37.6	1.09
RL27A_HUMAN	60S ribosomal protein L27a OS=Homo sapiens GN=RPL27A PE=1 SV=2	16.6	165.6	3	20.9	1.09
RL7_HUMAN	60S ribosomal protein L7 OS=Homo sapiens GN=RPL7 PE=1 SV=1	29.2	101	3	14.1	1.09
PARK7_HUMAN	Protein deglycase DJ-1 OS=Homo sapiens GN=PARK7 PE=1 SV=2	19.9	159.2	5	25.4	1.09
TBB4B_HUMAN	Tubulin beta-4B chain OS=Homo sapiens GN=TUBB4B PE=1 SV=1	49.8	1063.7	28	58.9	1.09
EFTU_HUMAN	Elongation factor Tu, mitochondrial OS=Homo sapiens GN=TUFM PE=1 SV=2	49.5	407.5	14	34.1	1.09
S10AD_HUMAN	Protein S100-A13 OS=Homo sapiens GN=S100A13 PE=1 SV=1	11.5	37	1	12.2	1.09
RL18_HUMAN	60S ribosomal protein L18 OS=Homo sapiens GN=RPL18 PE=1 SV=2	21.6	164.5	5	30.9	1.09
RS9_HUMAN	40S ribosomal protein S9 OS=Homo sapiens GN=RPS9 PE=1 SV=3	22.6	116	4	16.5	1.09
HYEP_HUMAN	Epoxide hydrolase 1 OS=Homo sapiens GN=EPHX1 PE=1 SV=1	52.9	237.5	6	16.9	1.09
ACLY_HUMAN	ATP-citrate synthase OS=Homo sapiens GN=ACLY PE=1 SV=3	120.8	382.6	12	14.6	1.09
XRCC5_HUMAN	X-ray repair cross-complementing protein 5 OS=Homo sapiens GN=XRCC5 PE=1 SV=3	82.7	195	7	13.3	1.09
HSP7C_HUMAN	Heat shock cognate 71 kDa protein OS=Homo sapiens GN=HSPA8 PE=1 SV=1	70.9	916.9	27	49.2	1.08
EF1A1_HUMAN	Elongation factor 1-alpha 1 OS=Homo sapiens GN=EEF1A1 PE=1 SV=1	50.1	435.3	12	38.7	1.08
RL14_HUMAN	60S ribosomal protein L14 OS=Homo sapiens GN=RPL14 PE=1 SV=4	23.4	115.1	4	15.3	1.08
RM12_HUMAN	39S ribosomal protein L12, mitochondrial OS=Homo sapiens GN=MRPL12 PE=1 SV=2	21.3	121.1	3	29.8	1.08
MATR3_HUMAN	Matrin-3 OS=Homo sapiens GN=MATR3 PE=1 SV=2	94.6	283.2	8	10.7	1.08
CAZA2_HUMAN	F-actin-capping protein subunit alpha-2 OS=Homo sapiens GN=CAPZA2 PE=1	32.9	56.6	2	9.8	1.08

	SV=3					
AGR2_HUMAN	Anterior gradient protein 2 homolog OS=Homo sapiens GN=AGR2 PE=1 SV=1	20	327.2	8	36	1.08
RS8_HUMAN	40S ribosomal protein S8 OS=Homo sapiens GN=RPS8 PE=1 SV=2	24.2	93.4	3	13.5	1.07
AK1C3_HUMAN	Aldo-keto reductase family 1 member C3 OS=Homo sapiens GN=AKR1C3 PE=1 SV=4	36.8	568.1	16	42.4	1.07
1433Z_HUMAN	14-3-3 protein zeta/delta OS=Homo sapiens GN=YWHAZ PE=1 SV=1	27.7	340.8	10	46.1	1.07
PROF1_HUMAN	Profilin-1 OS=Homo sapiens GN=PFN1 PE=1 SV=2	15	477.6	13	70.7	1.07
RL4_HUMAN	60S ribosomal protein L4 OS=Homo sapiens GN=RPL4 PE=1 SV=5	47.7	244.5	7	20.8	1.07
RS10_HUMAN	40S ribosomal protein S10 OS=Homo sapiens GN=RPS10 PE=1 SV=1	18.9	147.2	3	19.4	1.07
OST48_HUMAN	Dolichyl-diphosphooligosaccharide--protein glycosyltransferase 48 kDa subunit OS=Homo sapiens GN=DDOST PE=1 SV=4	50.8	90.6	2	5.3	1.07
MAP4_HUMAN	Microtubule-associated protein 4 OS=Homo sapiens GN=MAP4 PE=1 SV=3	120.9	71.7	3	4.5	1.07
RS18_HUMAN	40S ribosomal protein S18 OS=Homo sapiens GN=RPS18 PE=1 SV=3	17.7	207.2	7	32.9	1.07
SQSTM_HUMAN	Sequestosome-1 OS=Homo sapiens GN=SQSTM1 PE=1 SV=1	47.7	104.7	4	15.5	1.07
STML2_HUMAN	Stomatin-like protein 2, mitochondrial OS=Homo sapiens GN=STOML2 PE=1 SV=1	38.5	109.8	4	19.7	1.07
ERO1A_HUMAN	ERO1-like protein alpha OS=Homo sapiens GN=ERO1A PE=1 SV=2	54.4	58.8	2	4.1	1.07
RL31_HUMAN	60S ribosomal protein L31 OS=Homo sapiens GN=RPL31 PE=1 SV=1	14.5	118	3	19.2	1.07
1433B_HUMAN	14-3-3 protein beta/alpha OS=Homo sapiens GN=YWHAB PE=1 SV=3	28.1	220.1	7	27.6	1.07
ANXA5_HUMAN	Annexin A5 OS=Homo sapiens GN=ANXA5 PE=1 SV=2	35.9	176.5	5	20.9	1.06
6PGD_HUMAN	6-phosphogluconate dehydrogenase, decarboxylating OS=Homo sapiens GN=PGD PE=1 SV=3	53.1	627.9	14	40.8	1.06
G3P_HUMAN	Glyceraldehyde-3-phosphate dehydrogenase OS=Homo sapiens GN=GAPDH PE=1 SV=3	36	1009	25	50.7	1.06
CISY_HUMAN	Citrate synthase, mitochondrial OS=Homo sapiens GN=CS PE=1 SV=2	51.7	130.4	3	7.7	1.06
HS90B_HUMAN	Heat shock protein HSP 90-beta OS=Homo sapiens GN=HSP90AB1 PE=1 SV=4	83.2	719	21	39.1	1.06
AR6P1_HUMAN	ADP-ribosylation factor-like protein 6-interacting protein 1 OS=Homo sapiens GN=ARL6IP1 PE=1 SV=2	23.3	39.3	1	4.9	1.06
DSRAD_HUMAN	Double-stranded RNA-specific adenosine deaminase OS=Homo sapiens GN=ADAR PE=1 SV=4	136	35.9	1	1	1.06
RL13_HUMAN	60S ribosomal protein L13 OS=Homo sapiens GN=RPL13 PE=1 SV=4	24.2	176.5	4	14.2	1.06
GSTP1_HUMAN	Glutathione S-transferase P OS=Homo sapiens GN=GSTP1 PE=1 SV=2	23.3	191.6	5	38.6	1.06
AATM_HUMAN	Aspartate aminotransferase, mitochondrial OS=Homo sapiens GN=GOT2 PE=1 SV=3	47.5	142.9	5	15.1	1.06
RS27A_HUMAN	Ubiquitin-40S ribosomal protein S27a OS=Homo sapiens GN=RPS27A PE=1 SV=2	18	162.9	6	42.3	1.06
ERP29_HUMAN	Endoplasmic reticulum resident protein 29 OS=Homo sapiens GN=ERP29 PE=1 SV=4	29	177.5	5	27.2	1.06

ARF3_HUMAN	ADP-ribosylation factor 3 OS=Homo sapiens GN=ARF3 PE=1 SV=2	20.6	92.5	3	17.7	1.06
H2A2B_HUMAN	Histone H2A type 2-B OS=Homo sapiens GN=HIST2H2AB PE=1 SV=3	14	289.5	5	57.7	1.06
CN166_HUMAN	UPF0568 protein C14orf166 OS=Homo sapiens GN=C14orf166 PE=1 SV=1	28.1	145	5	27.9	1.06
RS16_HUMAN	40S ribosomal protein S16 OS=Homo sapiens GN=RPS16 PE=1 SV=2	16.4	112.2	4	26.7	1.05
HNRPF_HUMAN	Heterogeneous nuclear ribonucleoprotein F OS=Homo sapiens GN=HNRNPF PE=1 SV=3	45.6	183.3	5	16.9	1.05
STIP1_HUMAN	Stress-induced-phosphoprotein 1 OS=Homo sapiens GN=STIP1 PE=1 SV=1	62.6	195.6	7	15.5	1.05
TPIS_HUMAN	Triosephosphate isomerase OS=Homo sapiens GN=TPI1 PE=1 SV=3	30.8	459.3	9	47.6	1.05
RS25_HUMAN	40S ribosomal protein S25 OS=Homo sapiens GN=RPS25 PE=1 SV=1	13.7	125.4	4	31.2	1.05
AK1BA_HUMAN	Aldo-keto reductase family 1 member B10 OS=Homo sapiens GN=AKR1B10 PE=1 SV=2	36	610.7	14	38.6	1.05
CALM_HUMAN	Calmodulin OS=Homo sapiens GN=CALM1 PE=1 SV=2	16.8	233.2	6	47.7	1.05
PHB_HUMAN	Prohibitin OS=Homo sapiens GN=PHB PE=1 SV=1	29.8	285.5	6	34.6	1.04
FLNA_HUMAN	Filamin-A OS=Homo sapiens GN=FLNA PE=1 SV=4	280.6	989.4	30	17.3	1.04
H12_HUMAN	Histone H1.2 OS=Homo sapiens GN=HIST1H1C PE=1 SV=2	21.4	263.4	8	27.2	1.04
HS71A_HUMAN	Heat shock 70 kDa protein 1A OS=Homo sapiens GN=HSPA1A PE=1 SV=1	70	809.2	19	38.1	1.04
NONO_HUMAN	Non-POU domain-containing octamer-binding protein OS=Homo sapiens GN=NONO PE=1 SV=4	54.2	409.9	11	16.8	1.04
LMNB1_HUMAN	Lamin-B1 OS=Homo sapiens GN=LMNB1 PE=1 SV=2	66.4	200.9	6	14	1.04
S10A6_HUMAN	Protein S100-A6 OS=Homo sapiens GN=S100A6 PE=1 SV=1	10.2	108.2	3	16.7	1.04
MDHM_HUMAN	Malate dehydrogenase, mitochondrial OS=Homo sapiens GN=MDH2 PE=1 SV=3	35.5	567.8	15	56.2	1.04
PPIB_HUMAN	Peptidyl-prolyl cis-trans isomerase B OS=Homo sapiens GN=PPIB PE=1 SV=2	23.7	258.8	8	26.9	1.04
CH60_HUMAN	60 kDa heat shock protein, mitochondrial OS=Homo sapiens GN=HSPD1 PE=1 SV=2	61	1608.9	36	61.1	1.04
AHNK_HUMAN	Neuroblast differentiation-associated protein AHNAK OS=Homo sapiens GN=AHNAK PE=1 SV=2	628.7	330.3	12	2.9	1.04
H2AV_HUMAN	Histone H2A.V OS=Homo sapiens GN=H2AFV PE=1 SV=3	13.5	161	4	31.2	1.04
PFKAP_HUMAN	ATP-dependent 6-phosphofructokinase, platelet type OS=Homo sapiens GN=PFKP PE=1 SV=2	85.5	76.3	2	5	1.04
H4_HUMAN	Histone H4 OS=Homo sapiens GN=HIST1H4A PE=1 SV=2	11.4	493.6	12	58.3	1.04
PPIA_HUMAN	Peptidyl-prolyl cis-trans isomerase A OS=Homo sapiens GN=PPIA PE=1 SV=2	18	520.8	11	47.3	1.04
RPN1_HUMAN	Dolichyl-diphosphooligosaccharide--protein glycosyltransferase subunit 1 OS=Homo sapiens GN=RPN1 PE=1 SV=1	68.5	157.2	5	10	1.04
ASPH_HUMAN	Aspartyl/asparaginyl beta-hydroxylase OS=Homo sapiens GN=ASPH PE=1 SV=3	85.8	80.1	3	5.3	1.04
ITB1_HUMAN	Integrin beta-1 OS=Homo sapiens GN=ITGB1 PE=1 SV=2	88.4	203.1	7	11.4	1.03
S10AA_HUMAN	Protein S100-A10 OS=Homo sapiens	11.2	40.9	1	17.5	1.03

	GN=S100A10 PE=1 SV=2					
RS2_HUMAN	40S ribosomal protein S2 OS=Homo sapiens GN=RPS2 PE=1 SV=2	31.3	181.8	5	20.1	1.03
PDXK_HUMAN	Pyridoxal kinase OS=Homo sapiens GN=PDXK PE=1 SV=1	35.1	67.2	2	11.5	1.03
RAB7A_HUMAN	Ras-related protein Rab-7a OS=Homo sapiens GN=RAB7A PE=1 SV=1	23.5	120.3	4	28.5	1.03
VDAC1_HUMAN	Voltage-dependent anion-selective channel protein 1 OS=Homo sapiens GN=VDAC1 PE=1 SV=2	30.8	158.3	5	23.7	1.03
RL17_HUMAN	60S ribosomal protein L17 OS=Homo sapiens GN=RPL17 PE=1 SV=3	21.4	125	3	14.1	1.03
AK1C2_HUMAN	Aldo-keto reductase family 1 member C2 OS=Homo sapiens GN=AKR1C2 PE=1 SV=3	36.7	516.2	18	51.1	1.03
RS5_HUMAN	40S ribosomal protein S5 OS=Homo sapiens GN=RPS5 PE=1 SV=4	22.9	198.4	4	18.6	1.03
THIO_HUMAN	Thioredoxin OS=Homo sapiens GN=TXN PE=1 SV=3	11.7	173.1	4	38.1	1.03
ML12B_HUMAN	Myosin regulatory light chain 12B OS=Homo sapiens GN=MYL12B PE=1 SV=2	19.8	82.8	3	26.2	1.03
ANXA1_HUMAN	Annexin A1 OS=Homo sapiens GN=ANXA1 PE=1 SV=2	38.7	540.9	11	39.6	1.03
RSSA_HUMAN	40S ribosomal protein SA OS=Homo sapiens GN=RPSA PE=1 SV=4	32.8	166	4	17.6	1.03
ECHA_HUMAN	Trifunctional enzyme subunit alpha, mitochondrial OS=Homo sapiens GN=HADHA PE=1 SV=2	82.9	301.3	10	19.9	1.03
ALDR_HUMAN	Aldose reductase OS=Homo sapiens GN=AKR1B1 PE=1 SV=3	35.8	166.7	7	18	1.03
GSHR_HUMAN	Glutathione reductase, mitochondrial OS=Homo sapiens GN=GSR PE=1 SV=2	56.2	65.9	2	5	1.02
RTN4_HUMAN	Reticulon-4 OS=Homo sapiens GN=RTN4 PE=1 SV=2	129.9	173.3	4	6	1.02
HP1B3_HUMAN	Heterochromatin protein 1-binding protein 3 OS=Homo sapiens GN=HP1BP3 PE=1 SV=1	61.2	112.7	4	9	1.02
RBP56_HUMAN	TATA-binding protein-associated factor 2N OS=Homo sapiens GN=TAF15 PE=1 SV=1	61.8	93.3	3	5.2	1.02
GRP78_HUMAN	78 kDa glucose-regulated protein OS=Homo sapiens GN=HSPA5 PE=1 SV=2	72.3	896	21	33.9	1.02
GRP75_HUMAN	Stress-70 protein, mitochondrial OS=Homo sapiens GN=HSPA9 PE=1 SV=2	73.6	911.3	21	35.5	1.02
HINT2_HUMAN	Histidine triad nucleotide-binding protein 2, mitochondrial OS=Homo sapiens GN=HINT2 PE=1 SV=1	17.2	128.5	4	41.7	1.02
F136A_HUMAN	Protein FAM136A OS=Homo sapiens GN=FAM136A PE=1 SV=1	15.6	40.6	1	13	1.02
1433E_HUMAN	14-3-3 protein epsilon OS=Homo sapiens GN=YWHAE PE=1 SV=1	29.2	286.7	8	27.8	1.02
MIC60_HUMAN	MICOS complex subunit MIC60 OS=Homo sapiens GN=IMMT PE=1 SV=1	83.6	75.2	3	4.6	1.02
MVP_HUMAN	Major vault protein OS=Homo sapiens GN=MVP PE=1 SV=4	99.3	141.4	5	7.4	1.02
ANXA2_HUMAN	Annexin A2 OS=Homo sapiens GN=ANXA2 PE=1 SV=2	38.6	1002.2	27	61.9	1.02
1433G_HUMAN	14-3-3 protein gamma OS=Homo sapiens GN=YWHAG PE=1 SV=2	28.3	208.3	7	24.3	1.02
CYB5B_HUMAN	Cytochrome b5 type B OS=Homo sapiens GN=CYB5B PE=1 SV=2	16.3	148.7	4	14.4	1.02
BLVRB_HUMAN	Flavin reductase (NADPH) OS=Homo	22.1	121.1	4	23.8	1.02

	sapiens GN=BLVRB PE=1 SV=3					
HNRPC_HUMAN	Heterogeneous nuclear ribonucleoproteins C1/C2 OS=Homo sapiens GN=HNRNPC PE=1 SV=4	33.6	327.5	8	24.5	1.02
DDX24_HUMAN	ATP-dependent RNA helicase DDX24 OS=Homo sapiens GN=DDX24 PE=1 SV=1	96.3	84.4	2	4.3	1.01
H2AJ_HUMAN	Histone H2A.J OS=Homo sapiens GN=H2AFJ PE=1 SV=1	14	300.6	6	60.5	1.01
TLN1_HUMAN	Talin-1 OS=Homo sapiens GN=TLN1 PE=1 SV=3	269.6	183.8	6	3.8	1.01
PCBP1_HUMAN	Poly(rC)-binding protein 1 OS=Homo sapiens GN=PCBP1 PE=1 SV=2	37.5	255.9	8	24.2	1.01
PRDX1_HUMAN	Peroxiredoxin-1 OS=Homo sapiens GN=PRDX1 PE=1 SV=1	22.1	365.8	10	50.8	1.01
DDX3X_HUMAN	ATP-dependent RNA helicase DDX3X OS=Homo sapiens GN=DDX3X PE=1 SV=3	73.2	181.9	7	12.5	1.01
EF1G_HUMAN	Elongation factor 1-gamma OS=Homo sapiens GN=EEF1G PE=1 SV=3	50.1	127.5	4	12.4	1.01
ETFB_HUMAN	Electron transfer flavoprotein subunit beta OS=Homo sapiens GN=ETFB PE=1 SV=3	27.8	163.5	7	26.3	1.01
KPYM_HUMAN	Pyruvate kinase PKM OS=Homo sapiens GN=PKM PE=1 SV=4	57.9	1220.8	31	61.4	1.01
H2A2C_HUMAN	Histone H2A type 2-C OS=Homo sapiens GN=HIST2H2AC PE=1 SV=4	14	377	7	60.5	1.01
LYRIC_HUMAN	Protein LYRIC OS=Homo sapiens GN=MTDH PE=1 SV=2	63.8	59.3	2	4	1.01
RLA2_HUMAN	60S acidic ribosomal protein P2 OS=Homo sapiens GN=RPLP2 PE=1 SV=1	11.7	144.1	4	69.6	1.01
AL1B1_HUMAN	Aldehyde dehydrogenase X, mitochondrial OS=Homo sapiens GN=ALDH1B1 PE=1 SV=3	57.2	137.2	5	13.9	1.01
ADT3_HUMAN	ADP/ATP translocase 3 OS=Homo sapiens GN=SLC25A6 PE=1 SV=4	32.8	405	12	44	1.01
IQGA1_HUMAN	Ras GTPase-activating-like protein IQGAP1 OS=Homo sapiens GN=IQGAP1 PE=1 SV=1	189.1	150.9	4	4.5	1.01
COX5B_HUMAN	Cytochrome c oxidase subunit 5B, mitochondrial OS=Homo sapiens GN=COX5B PE=1 SV=2	13.7	81.1	3	24	1.01
SMD1_HUMAN	Small nuclear ribonucleoprotein Sm D1 OS=Homo sapiens GN=SNRPD1 PE=1 SV=1	13.3	64.9	2	27.7	1.01
PP1G_HUMAN	Serine/threonine-protein phosphatase PP1-gamma catalytic subunit OS=Homo sapiens GN=PPP1CC PE=1 SV=1	37	53.6	2	8.7	1.01
MYH9_HUMAN	Myosin-9 OS=Homo sapiens GN=MYH9 PE=1 SV=4	226.4	927.7	28	18.7	1.00
PGK1_HUMAN	Phosphoglycerate kinase 1 OS=Homo sapiens GN=PGK1 PE=1 SV=3	44.6	347.3	9	28.3	1.00
RL23_HUMAN	60S ribosomal protein L23 OS=Homo sapiens GN=RPL23 PE=1 SV=1	14.9	132.1	4	31.4	1.00
RL15_HUMAN	60S ribosomal protein L15 OS=Homo sapiens GN=RPL15 PE=1 SV=2	24.1	56	2	10.3	1.00
G6PD_HUMAN	Glucose-6-phosphate 1-dehydrogenase OS=Homo sapiens GN=G6PD PE=1 SV=4	59.2	791.7	25	48.9	1.00
TERA_HUMAN	Transitional endoplasmic reticulum ATPase OS=Homo sapiens GN=VCP PE=1 SV=4	89.3	554.8	18	28.7	1.00
TPM3_HUMAN	Tropomyosin alpha-3 chain OS=Homo sapiens GN=TPM3 PE=1 SV=2	32.9	113.6	3	11.6	1.00
COX5A_HUMAN	Cytochrome c oxidase subunit 5A, mitochondrial OS=Homo sapiens GN=COX5A PE=1 SV=2	16.8	83	3	25.3	1.00

TCPA_HUMAN	T-complex protein 1 subunit alpha OS=Homo sapiens GN=TCP1 PE=1 SV=1	60.3	111.5	5	10.4	1.00
ACTN1_HUMAN	Alpha-actinin-1 OS=Homo sapiens GN=ACTN1 PE=1 SV=2	103	455.8	14	19.7	1.00
PDIA6_HUMAN	Protein disulfide-isomerase A6 OS=Homo sapiens GN=PDIA6 PE=1 SV=1	48.1	354.2	8	32.3	1.00
CALR_HUMAN	Calreticulin OS=Homo sapiens GN=CALR PE=1 SV=1	48.1	264	10	33.1	1.00
CH10_HUMAN	10 kDa heat shock protein, mitochondrial OS=Homo sapiens GN=HSPE1 PE=1 SV=2	10.9	258.5	7	66.7	1.00
AL3A1_HUMAN	Aldehyde dehydrogenase, dimeric NADP-preferring OS=Homo sapiens GN=ALDH3A1 PE=1 SV=3	50.4	360.2	9	25.4	1.00
RS3A_HUMAN	40S ribosomal protein S3a OS=Homo sapiens GN=RPS3A PE=1 SV=2	29.9	160.5	4	16.7	1.00
PDIA1_HUMAN	Protein disulfide-isomerase OS=Homo sapiens GN=P4HB PE=1 SV=3	57.1	631.7	18	33.5	0.99
CALX_HUMAN	Calnexin OS=Homo sapiens GN=CANX PE=1 SV=2	67.5	406.8	10	17.9	0.99
TPM4_HUMAN	Tropomyosin alpha-4 chain OS=Homo sapiens GN=TPM4 PE=1 SV=3	28.5	100.4	2	8.1	0.99
HNRPQ_HUMAN	Heterogeneous nuclear ribonucleoprotein Q OS=Homo sapiens GN=SYNCRIP PE=1 SV=2	69.6	262.9	7	13.6	0.99
LDHA_HUMAN	L-lactate dehydrogenase A chain OS=Homo sapiens GN=LDHA PE=1 SV=2	36.7	436.4	12	43.4	0.99
ACTG_HUMAN	Actin, cytoplasmic 2 OS=Homo sapiens GN=ACTG1 PE=1 SV=1	41.8	1514.5	34	60.8	0.99
H2B1K_HUMAN	Histone H2B type 1-K OS=Homo sapiens GN=HIST1H2BK PE=1 SV=3	13.9	622	13	53.2	0.99
ROA1_HUMAN	Heterogeneous nuclear ribonucleoprotein A1 OS=Homo sapiens GN=HNRNPA1 PE=1 SV=5	38.7	668.1	16	31.2	0.99
RL36_HUMAN	60S ribosomal protein L36 OS=Homo sapiens GN=RPL36 PE=1 SV=3	12.2	119.2	3	21	0.99
AIFM1_HUMAN	Apoptosis-inducing factor 1, mitochondrial OS=Homo sapiens GN=AIFM1 PE=1 SV=1	66.9	91.5	2	5.4	0.99
RHOA_HUMAN	Transforming protein RhoA OS=Homo sapiens GN=RHOA PE=1 SV=1	21.8	50.9	2	13	0.99
RBMX_HUMAN	RNA-binding motif protein, X chromosome OS=Homo sapiens GN=RBMX PE=1 SV=3	42.3	147.6	5	11	0.99
MIF_HUMAN	Macrophage migration inhibitory factor OS=Homo sapiens GN=MIF PE=1 SV=4	12.5	57.8	2	17.4	0.99
CKAP4_HUMAN	Cytoskeleton-associated protein 4 OS=Homo sapiens GN=CKAP4 PE=1 SV=2	66	324.2	9	21.8	0.99
PA1B3_HUMAN	Platelet-activating factor acetylhydrolase IB subunit gamma OS=Homo sapiens GN=PAFAH1B3 PE=1 SV=1	25.7	64.8	2	11.3	0.99
ANXA4_HUMAN	Annexin A4 OS=Homo sapiens GN=ANXA4 PE=1 SV=4	35.9	236.4	7	29.2	0.99
ROA2_HUMAN	Heterogeneous nuclear ribonucleoproteins A2/B1 OS=Homo sapiens GN=HNRNPA2B1 PE=1 SV=2	37.4	610.9	19	44.8	0.99
PSMD2_HUMAN	26S proteasome non-ATPase regulatory subunit 2 OS=Homo sapiens GN=PSMD2 PE=1 SV=3	100.1	111.3	2	4.1	0.98
PGRC2_HUMAN	Membrane-associated progesterone receptor component 2 OS=Homo sapiens GN=PGRMC2 PE=1 SV=1	23.8	124	2	12.6	0.98
SAP_HUMAN	Prosaposin OS=Homo sapiens GN=PSAP PE=1 SV=2	58.1	146.3	6	12.2	0.98

PRKDC_HUMAN	DNA-dependent protein kinase catalytic subunit OS=Homo sapiens GN=PRKDC PE=1 SV=3	468.8	486	20	6.2	0.98
CALU_HUMAN	Calumenin OS=Homo sapiens GN=CALU PE=1 SV=2	37.1	86.6	3	13.3	0.98
LONM_HUMAN	Lon protease homolog, mitochondrial OS=Homo sapiens GN=LONP1 PE=1 SV=2	106.4	96.2	4	7.4	0.98
PRDX3_HUMAN	Thioredoxin-dependent peroxide reductase, mitochondrial OS=Homo sapiens GN=PRDX3 PE=1 SV=3	27.7	103.2	2	10.2	0.98
ALDH2_HUMAN	Aldehyde dehydrogenase, mitochondrial OS=Homo sapiens GN=ALDH2 PE=1 SV=2	56.3	181.9	7	16.1	0.98
SFPQ_HUMAN	Splicing factor, proline- and glutamine-rich OS=Homo sapiens GN=SFPQ PE=1 SV=2	76.1	171.3	6	6.6	0.98
RCN1_HUMAN	Reticulocalbin-1 OS=Homo sapiens GN=RCN1 PE=1 SV=1	38.9	90.9	3	9.4	0.98
ACTC_HUMAN	Actin, alpha cardiac muscle 1 OS=Homo sapiens GN=ACTC1 PE=1 SV=1	42	844.3	21	37.4	0.98
ROA3_HUMAN	Heterogeneous nuclear ribonucleoprotein A3 OS=Homo sapiens GN=HNRNPA3 PE=1 SV=2	39.6	226.2	6	15.6	0.98
NPM_HUMAN	Nucleophosmin OS=Homo sapiens GN=NPM1 PE=1 SV=2	32.6	612.8	11	30.6	0.98
HNRH1_HUMAN	Heterogeneous nuclear ribonucleoprotein H OS=Homo sapiens GN=HNRNPH1 PE=1 SV=4	49.2	255.4	7	23.2	0.98
PHS_HUMAN	Pterin-4-alpha-carbinolamine dehydratase OS=Homo sapiens GN=PCBD1 PE=1 SV=2	12	66	2	15.4	0.98
UGDH_HUMAN	UDP-glucose 6-dehydrogenase OS=Homo sapiens GN=UGDH PE=1 SV=1	55	469.2	14	40.5	0.98
H2B1B_HUMAN	Histone H2B type 1-B OS=Homo sapiens GN=HIST1H2BB PE=1 SV=2	13.9	589.1	12	53.2	0.98
AL1A1_HUMAN	Retinal dehydrogenase 1 OS=Homo sapiens GN=ALDH1A1 PE=1 SV=2	54.8	1157.1	29	52.3	0.98
BAF_HUMAN	Barrier-to-autointegration factor OS=Homo sapiens GN=BANF1 PE=1 SV=1	10.1	143.1	5	56.2	0.98
COF1_HUMAN	Cofilin-1 OS=Homo sapiens GN=CFL1 PE=1 SV=3	18.5	226.1	6	50.6	0.98
H33_HUMAN	Histone H3.3 OS=Homo sapiens GN=H3F3A PE=1 SV=2	15.3	89.9	3	16.9	0.98
HCD2_HUMAN	3-hydroxyacyl-CoA dehydrogenase type-2 OS=Homo sapiens GN=HSD17B10 PE=1 SV=3	26.9	124	5	24.5	0.98
HNRDL_HUMAN	Heterogeneous nuclear ribonucleoprotein D-like OS=Homo sapiens GN=HNRNPDL PE=1 SV=3	46.4	89.8	3	7.1	0.98
FLNB_HUMAN	Filamin-B OS=Homo sapiens GN=FLNB PE=1 SV=2	278	825.7	25	13.5	0.98
DHX9_HUMAN	ATP-dependent RNA helicase A OS=Homo sapiens GN=DHX9 PE=1 SV=4	140.9	407.7	14	13.7	0.97
ACADV_HUMAN	Very long-chain specific acyl-CoA dehydrogenase, mitochondrial OS=Homo sapiens GN=ACADVL PE=1 SV=1	70.3	65.8	2	4	0.97
RS6_HUMAN	40S ribosomal protein S6 OS=Homo sapiens GN=RPS6 PE=1 SV=1	28.7	124.9	5	19.3	0.97
MYL6_HUMAN	Myosin light polypeptide 6 OS=Homo sapiens GN=MYL6 PE=1 SV=2	16.9	162.8	6	39.1	0.97
DDX5_HUMAN	Probable ATP-dependent RNA helicase DDX5 OS=Homo sapiens GN=DDX5 PE=1 SV=1	69.1	167.6	5	10.3	0.97
SPTN1_HUMAN	Spectrin alpha chain, non-erythrocytic 1 OS=Homo sapiens GN=SPTAN1 PE=1	284.4	425.7	15	7.4	0.97

	SV=3					
PHB2_HUMAN	Prohibitin-2 OS=Homo sapiens GN=PHB2 PE=1 SV=2	33.3	335.3	9	37.1	0.97
SRSF1_HUMAN	Serine/arginine-rich splicing factor 1 OS=Homo sapiens GN=SRSF1 PE=1 SV=2	27.7	85.4	4	15.7	0.97
RL3_HUMAN	60S ribosomal protein L3 OS=Homo sapiens GN=RPL3 PE=1 SV=2	46.1	147.5	6	18.4	0.97
MPRD_HUMAN	Cation-dependent mannose-6-phosphate receptor OS=Homo sapiens GN=M6PR PE=1 SV=1	31	36.4	1	7.6	0.97
HNRPR_HUMAN	Heterogeneous nuclear ribonucleoprotein R OS=Homo sapiens GN=HNRNPR PE=1 SV=1	70.9	152.1	6	8.1	0.97
CD44_HUMAN	CD44 antigen OS=Homo sapiens GN=CD44 PE=1 SV=3	81.5	235	5	6.3	0.97
ATPB_HUMAN	ATP synthase subunit beta, mitochondrial OS=Homo sapiens GN=ATP5B PE=1 SV=3	56.5	814.7	24	45.9	0.97
PCBP2_HUMAN	Poly(rC)-binding protein 2 OS=Homo sapiens GN=PCBP2 PE=1 SV=1	38.6	243.4	8	22.5	0.97
IF5A1_HUMAN	Eukaryotic translation initiation factor 5A-1 OS=Homo sapiens GN=EIF5A PE=1 SV=2	16.8	91.6	2	23.4	0.97
PTBP1_HUMAN	Polypyrimidine tract-binding protein 1 OS=Homo sapiens GN=PTBP1 PE=1 SV=1	57.2	219.6	4	15.4	0.97
LEG1_HUMAN	Galectin-1 OS=Homo sapiens GN=LGALS1 PE=1 SV=2	14.7	86.4	3	26.7	0.97
U520_HUMAN	U5 small nuclear ribonucleoprotein 200 kDa helicase OS=Homo sapiens GN=SNRNP200 PE=1 SV=2	244.4	113.9	4	2.4	0.97
RL10_HUMAN	60S ribosomal protein L10 OS=Homo sapiens GN=RPL10 PE=1 SV=4	24.6	134.5	5	27.6	0.97
SSBP_HUMAN	Single-stranded DNA-binding protein, mitochondrial OS=Homo sapiens GN=SSBP1 PE=1 SV=1	17.2	98.4	2	22.3	0.96
LMNA_HUMAN	Prelamin-A/C OS=Homo sapiens GN=LMNA PE=1 SV=1	74.1	672.8	20	34	0.96
TKT_HUMAN	Transketolase OS=Homo sapiens GN=TKT PE=1 SV=3	67.8	692.8	17	29.5	0.96
ATPA_HUMAN	ATP synthase subunit alpha, mitochondrial OS=Homo sapiens GN=ATP5A1 PE=1 SV=1	59.7	763	19	39.1	0.96
EF1D_HUMAN	Elongation factor 1-delta OS=Homo sapiens GN=EEF1D PE=1 SV=5	31.1	157.6	4	17.4	0.96
COX2_HUMAN	Cytochrome c oxidase subunit 2 OS=Homo sapiens GN=MT-CO2 PE=1 SV=1	25.5	35.4	1	4.4	0.96
SYMC_HUMAN	Methionine--tRNA ligase, cytoplasmic OS=Homo sapiens GN=MARS PE=1 SV=2	101.1	81.1	3	4.4	0.96
IF2A_HUMAN	Eukaryotic translation initiation factor 2 subunit 1 OS=Homo sapiens GN=EIF2S1 PE=1 SV=3	36.1	60.1	2	7	0.96
RS28_HUMAN	40S ribosomal protein S28 OS=Homo sapiens GN=RPS28 PE=1 SV=1	7.8	73.4	2	30.4	0.96
PSB1_HUMAN	Proteasome subunit beta type-1 OS=Homo sapiens GN=PSMB1 PE=1 SV=2	26.5	82	2	13.3	0.96
LDHB_HUMAN	L-lactate dehydrogenase B chain OS=Homo sapiens GN=LDHB PE=1 SV=2	36.6	329.9	9	28.4	0.96
CLH1_HUMAN	Clathrin heavy chain 1 OS=Homo sapiens GN=CLTC PE=1 SV=5	191.5	883.1	28	21.1	0.96
NDUS1_HUMAN	NADH-ubiquinone oxidoreductase 75 kDa subunit, mitochondrial OS=Homo sapiens GN=NDUFS1 PE=1 SV=3	79.4	37.8	1	2.1	0.96

RL6_HUMAN	60S ribosomal protein L6 OS=Homo sapiens GN=RPL6 PE=1 SV=3	32.7	254.4	7	21.5	0.95
C1QBP_HUMAN	Complement component 1 Q subcomponent-binding protein, mitochondrial OS=Homo sapiens GN=C1QBP PE=1 SV=1	31.3	381.3	9	40.8	0.95
KHDR1_HUMAN	KH domain-containing, RNA-binding, signal transduction-associated protein 1 OS=Homo sapiens GN=KHDRBS1 PE=1 SV=1	48.2	63.2	2	6.5	0.95
ILF2_HUMAN	Interleukin enhancer-binding factor 2 OS=Homo sapiens GN=ILF2 PE=1 SV=2	43	184	6	22.1	0.95
TCPB_HUMAN	T-complex protein 1 subunit beta OS=Homo sapiens GN=CCT2 PE=1 SV=4	57.5	340.8	8	21.1	0.95
CDC42_HUMAN	Cell division control protein 42 homolog OS=Homo sapiens GN=CDC42 PE=1 SV=2	21.2	115.6	3	20.9	0.95
HNRPK_HUMAN	Heterogeneous nuclear ribonucleoprotein K OS=Homo sapiens GN=HNRNPK PE=1 SV=1	50.9	511.9	16	36.7	0.95
PON2_HUMAN	Serum paraoxonase/arylesterase 2 OS=Homo sapiens GN=PON2 PE=1 SV=3	39.4	93.5	3	11.9	0.95
VIME_HUMAN	Vimentin OS=Homo sapiens GN=VIM PE=1 SV=4	53.6	1394.8	34	56.7	0.95
RAB1C_HUMAN	Putative Ras-related protein Rab-1C OS=Homo sapiens GN=RAB1C PE=5 SV=2	22	132.2	4	22.9	0.95
GDIB_HUMAN	Rab GDP dissociation inhibitor beta OS=Homo sapiens GN=GDI2 PE=1 SV=2	50.6	37.3	1	2.5	0.94
TBA1B_HUMAN	Tubulin alpha-1B chain OS=Homo sapiens GN=TUBA1B PE=1 SV=1	50.1	803.8	17	45.5	0.94
SFXN3_HUMAN	Sideroflexin-3 OS=Homo sapiens GN=SFXN3 PE=1 SV=2	36	94	3	10.5	0.94
PTMS_HUMAN	Parathymosin OS=Homo sapiens GN=PTMS PE=1 SV=2	11.5	52.2	1	10.8	0.94
TBA1C_HUMAN	Tubulin alpha-1C chain OS=Homo sapiens GN=TUBA1C PE=1 SV=1	49.9	673.8	16	41	0.93
SRSF2_HUMAN	Serine/arginine-rich splicing factor 2 OS=Homo sapiens GN=SRSF2 PE=1 SV=4	25.5	182.8	5	11.8	0.93
PLEC_HUMAN	Plectin OS=Homo sapiens GN=PLEC PE=1 SV=3	531.5	1789.8	59	17.3	0.93
ECH1_HUMAN	Delta(3,5)-Delta(2,4)-dienoyl-CoA isomerase, mitochondrial OS=Homo sapiens GN=ECH1 PE=1 SV=2	35.8	273.1	7	23.8	0.93
LRC59_HUMAN	Leucine-rich repeat-containing protein 59 OS=Homo sapiens GN=LRRC59 PE=1 SV=1	34.9	236.1	6	25.7	0.93
K2C1_HUMAN	Keratin, type II cytoskeletal 1 OS=Homo sapiens GN=KRT1 PE=1 SV=6	66	202.7	5	5.9	0.93
HNRPD_HUMAN	Heterogeneous nuclear ribonucleoprotein D0 OS=Homo sapiens GN=HNRNPD PE=1 SV=1	38.4	168.2	6	20	0.93
ALDOA_HUMAN	Fructose-bisphosphate aldolase A OS=Homo sapiens GN=ALDOA PE=1 SV=2	39.4	402.6	9	31.6	0.93
HNRPU_HUMAN	Heterogeneous nuclear ribonucleoprotein U OS=Homo sapiens GN=HNRNPU PE=1 SV=6	90.5	398.3	13	20.4	0.93
ENOA_HUMAN	Alpha-enolase OS=Homo sapiens GN=ENO1 PE=1 SV=2	47.1	1274.7	26	64.5	0.93
NCPR_HUMAN	NADPH--cytochrome P450 reductase OS=Homo sapiens GN=POR PE=1 SV=2	76.6	146.1	5	13.3	0.93
ADT2_HUMAN	ADP/ATP translocase 2 OS=Homo sapiens GN=SLC25A5 PE=1 SV=7	32.8	422.1	13	35.2	0.93
KAD3_HUMAN	GTP:AMP phosphotransferase AK3,	25.5	61	2	11	0.93

	mitochondrial OS=Homo sapiens GN=AK3 PE=1 SV=4					
ODPB_HUMAN	Pyruvate dehydrogenase E1 component subunit beta, mitochondrial OS=Homo sapiens GN=PDHB PE=1 SV=3	39.2	56.4	2	8.9	0.93
TCPE_HUMAN	T-complex protein 1 subunit epsilon OS=Homo sapiens GN=CCT5 PE=1 SV=1	59.6	162	7	15.3	0.93
NDUA9_HUMAN	NADH dehydrogenase [ubiquinone] 1 alpha subcomplex subunit 9, mitochondrial OS=Homo sapiens GN=NDUFA9 PE=1 SV=2	42.5	115.1	4	17.2	0.92
ECHM_HUMAN	Enoyl-CoA hydratase, mitochondrial OS=Homo sapiens GN=ECHS1 PE=1 SV=4	31.4	73.5	2	13.1	0.92
NDUA4_HUMAN	Cytochrome c oxidase subunit NDUFA4 OS=Homo sapiens GN=NDUFA4 PE=1 SV=1	9.4	33.3	1	14.8	0.92
CTND1_HUMAN	Catenin delta-1 OS=Homo sapiens GN=CTNND1 PE=1 SV=1	108.1	119.5	2	2.9	0.92
TBA1A_HUMAN	Tubulin alpha-1A chain OS=Homo sapiens GN=TUBA1A PE=1 SV=1	50.1	809.6	17	45.5	0.92
CATD_HUMAN	Cathepsin D OS=Homo sapiens GN=CTSD PE=1 SV=1	44.5	149.3	6	22.1	0.92
RS3_HUMAN	40S ribosomal protein S3 OS=Homo sapiens GN=RPS3 PE=1 SV=2	26.7	102.3	4	17.3	0.92
S12A2_HUMAN	Solute carrier family 12 member 2 OS=Homo sapiens GN=SLC12A2 PE=1 SV=1	131.4	73	3	3.5	0.92
4F2_HUMAN	4F2 cell-surface antigen heavy chain OS=Homo sapiens GN=SLC3A2 PE=1 SV=3	68	457.4	12	25.4	0.92
ACTN4_HUMAN	Alpha-actinin-4 OS=Homo sapiens GN=ACTN4 PE=1 SV=2	104.8	798.1	25	33.9	0.92
RLA0_HUMAN	60S acidic ribosomal protein P0 OS=Homo sapiens GN=RPLP0 PE=1 SV=1	34.3	281.4	10	48.3	0.92
SQRD_HUMAN	Sulfide:quinone oxidoreductase, mitochondrial OS=Homo sapiens GN=SQRDL PE=1 SV=1	49.9	96.7	4	9.1	0.92
FAS_HUMAN	Fatty acid synthase OS=Homo sapiens GN=FASN PE=1 SV=3	273.3	469.1	18	8.6	0.92
QCR1_HUMAN	Cytochrome b-c1 complex subunit 1, mitochondrial OS=Homo sapiens GN=UQCRC1 PE=1 SV=3	52.6	137.6	5	16.7	0.92
COPG2_HUMAN	Coatomer subunit gamma-2 OS=Homo sapiens GN=COPG2 PE=1 SV=1	97.6	36.9	1	1.4	0.92
IF4A1_HUMAN	Eukaryotic initiation factor 4A-I OS=Homo sapiens GN=EIF4A1 PE=1 SV=1	46.1	223	7	17.7	0.91
K2C7_HUMAN	Keratin, type II cytoskeletal 7 OS=Homo sapiens GN=KRT7 PE=1 SV=5	51.4	940.1	24	49.5	0.91
GCN1_HUMAN	eIF-2-alpha kinase activator GCN1 OS=Homo sapiens GN=GCN1 PE=1 SV=6	292.6	128.2	4	3	0.91
LAMP1_HUMAN	Lysosome-associated membrane glycoprotein 1 OS=Homo sapiens GN=LAMP1 PE=1 SV=3	44.9	34.5	1	2.2	0.90
ETFA_HUMAN	Electron transfer flavoprotein subunit alpha, mitochondrial OS=Homo sapiens GN=ETFA PE=1 SV=1	35.1	235.8	5	20.7	0.90
PGAM2_HUMAN	Phosphoglycerate mutase 2 OS=Homo sapiens GN=PGAM2 PE=1 SV=3	28.7	48.8	1	5.5	0.90
TCPH_HUMAN	T-complex protein 1 subunit eta OS=Homo sapiens GN=CCT7 PE=1 SV=2	59.3	96.8	3	7.2	0.90
MCM7_HUMAN	DNA replication licensing factor MCM7 OS=Homo sapiens GN=MCM7 PE=1 SV=4	81.3	67	2	4	0.90
YBOX1_HUMAN	Nuclease-sensitive element-binding protein	35.9	85.6	2	11.1	0.90

	1 OS=Homo sapiens GN=YBX1 PE=1 SV=3					
RS20_HUMAN	40S ribosomal protein S20 OS=Homo sapiens GN=RPS20 PE=1 SV=1	13.4	135.7	4	42	0.90
UBA1_HUMAN	Ubiquitin-like modifier-activating enzyme 1 OS=Homo sapiens GN=UBA1 PE=1 SV=3	117.8	150.2	4	6.1	0.90
TALDO_HUMAN	Transaldolase OS=Homo sapiens GN=TALDO1 PE=1 SV=2	37.5	164.1	4	13.1	0.90
TCP4_HUMAN	Activated RNA polymerase II transcriptional coactivator p15 OS=Homo sapiens GN=SUB1 PE=1 SV=3	14.4	79.3	2	18.9	0.90
EZRI_HUMAN	Ezrin OS=Homo sapiens GN=EZR PE=1 SV=4	69.4	135.9	5	10.4	0.90
NUCL_HUMAN	Nucleolin OS=Homo sapiens GN=NCL PE=1 SV=3	76.6	451.4	15	20.1	0.89
CATB_HUMAN	Cathepsin B OS=Homo sapiens GN=CTSB PE=1 SV=3	37.8	121.1	3	10.3	0.89
TPM1_HUMAN	Tropomyosin alpha-1 chain OS=Homo sapiens GN=TPM1 PE=1 SV=2	32.7	89.8	2	7	0.89
K1C18_HUMAN	Keratin, type I cytoskeletal 18 OS=Homo sapiens GN=KRT18 PE=1 SV=2	48	1784.1	40	72.6	0.89
SYEP_HUMAN	Bifunctional glutamate/proline--tRNA ligase OS=Homo sapiens GN=EPRS PE=1 SV=5	170.5	84.9	3	2.5	0.88
KTN1_HUMAN	Kinectin OS=Homo sapiens GN=KTN1 PE=1 SV=1	156.2	136.1	4	4.9	0.88
MOES_HUMAN	Moesin OS=Homo sapiens GN=MSN PE=1 SV=3	67.8	135.6	4	8.3	0.88
GBLP_HUMAN	Guanine nucleotide-binding protein subunit beta-2-like 1 OS=Homo sapiens GN=GNB2L1 PE=1 SV=3	35.1	99.3	4	15.1	0.88
S10AB_HUMAN	Protein S100-A11 OS=Homo sapiens GN=S100A11 PE=1 SV=2	11.7	94.8	3	34.3	0.87
K2C8_HUMAN	Keratin, type II cytoskeletal 8 OS=Homo sapiens GN=KRT8 PE=1 SV=7	53.7	2083.5	44	70.4	0.87
EMC3_HUMAN	ER membrane protein complex subunit 3 OS=Homo sapiens GN=EMC3 PE=1 SV=3	29.9	38.6	1	5.4	0.87
DHE3_HUMAN	Glutamate dehydrogenase 1, mitochondrial OS=Homo sapiens GN=GLUD1 PE=1 SV=2	61.4	139.5	5	11.8	0.87
MYOF_HUMAN	Myoferlin OS=Homo sapiens GN=MYOF PE=1 SV=1	234.6	77.1	3	1.8	0.86
RS4X_HUMAN	40S ribosomal protein S4, X isoform OS=Homo sapiens GN=RPS4X PE=1 SV=2	29.6	180.7	7	26.2	0.86
OLA1_HUMAN	Obg-like ATPase 1 OS=Homo sapiens GN=OLA1 PE=1 SV=2	44.7	39.6	1	3.8	0.86
DHB4_HUMAN	Peroxisomal multifunctional enzyme type 2 OS=Homo sapiens GN=HSD17B4 PE=1 SV=3	79.6	35.8	1	2	0.86
FUBP2_HUMAN	Far upstream element-binding protein 2 OS=Homo sapiens GN=KHSRP PE=1 SV=4	73.1	91.1	3	4.5	0.86
TMEDA_HUMAN	Transmembrane emp24 domain-containing protein 10 OS=Homo sapiens GN=TMED10 PE=1 SV=2	25	118.7	4	26.5	0.86
CMC2_HUMAN	Calcium-binding mitochondrial carrier protein Aralar2 OS=Homo sapiens GN=SLC25A13 PE=1 SV=2	74.1	72.1	3	5.8	0.86
PAIRB_HUMAN	Plasminogen activator inhibitor 1 RNA-binding protein OS=Homo sapiens GN=SERBP1 PE=1 SV=2	44.9	106.6	3	12	0.86
IMB1_HUMAN	Importin subunit beta-1 OS=Homo sapiens GN=KPNB1 PE=1 SV=2	97.1	149.1	5	7.4	0.85

DYHC1_HUMAN	Cytoplasmic dynein 1 heavy chain 1 OS=Homo sapiens GN=DYNC1H1 PE=1 SV=5	532.1	179.1	7	2	0.85
SYAC_HUMAN	Alanine--tRNA ligase, cytoplasmic OS=Homo sapiens GN=AARS PE=1 SV=2	106.7	89.4	3	5	0.85
SPRE_HUMAN	Sepiapterin reductase OS=Homo sapiens GN=SPR PE=1 SV=1	28	39.7	1	7.3	0.85
SON_HUMAN	Protein SON OS=Homo sapiens GN=SON PE=1 SV=4	263.7	39.5	1	0.6	0.85
CBR1_HUMAN	Carbonyl reductase [NADPH] 1 OS=Homo sapiens GN=CBR1 PE=1 SV=3	30.4	90	3	13.4	0.84
XRCC6_HUMAN	X-ray repair cross-complementing protein 6 OS=Homo sapiens GN=XRCC6 PE=1 SV=2	69.8	423.6	12	26.1	0.84
K1C19_HUMAN	Keratin, type I cytoskeletal 19 OS=Homo sapiens GN=KRT19 PE=1 SV=4	44.1	389.9	11	27.5	0.84
ECHB_HUMAN	Trifunctional enzyme subunit beta, mitochondrial OS=Homo sapiens GN=HADHB PE=1 SV=3	51.3	204	6	13.1	0.84
SF3B6_HUMAN	Splicing factor 3B subunit 6 OS=Homo sapiens GN=SF3B6 PE=1 SV=1	14.6	33.2	1	11.2	0.84
RAB14_HUMAN	Ras-related protein Rab-14 OS=Homo sapiens GN=RAB14 PE=1 SV=4	23.9	55.5	2	11.6	0.84
RS23_HUMAN	40S ribosomal protein S23 OS=Homo sapiens GN=RPS23 PE=1 SV=3	15.8	94.4	3	23.1	0.83
PPIF_HUMAN	Peptidyl-prolyl cis-trans isomerase F, mitochondrial OS=Homo sapiens GN=PPIF PE=1 SV=1	22	39.8	1	4.8	0.83
CRIP1_HUMAN	Cysteine-rich protein 1 OS=Homo sapiens GN=CRIP1 PE=1 SV=3	8.5	46.1	2	20.8	0.82
DDX21_HUMAN	Nucleolar RNA helicase 2 OS=Homo sapiens GN=DDX21 PE=1 SV=5	87.3	59.8	2	3.4	0.82
LPPRC_HUMAN	Leucine-rich PPR motif-containing protein, mitochondrial OS=Homo sapiens GN=LRPPRC PE=1 SV=3	157.8	389.6	13	13	0.82
HACD3_HUMAN	Very-long-chain (3R)-3-hydroxyacyl-CoA dehydratase 3 OS=Homo sapiens GN=HACD3 PE=1 SV=2	43.1	34.6	1	3	0.82
FIS1_HUMAN	Mitochondrial fission 1 protein OS=Homo sapiens GN=FIS1 PE=1 SV=2	16.9	36.1	1	7.2	0.81
CNPY2_HUMAN	Protein canopy homolog 2 OS=Homo sapiens GN=CNPY2 PE=1 SV=1	20.6	59.5	1	8.8	0.81
LA_HUMAN	Lupus La protein OS=Homo sapiens GN=SSB PE=1 SV=2	46.8	85	3	9.3	0.81
PTRF_HUMAN	Polymerase I and transcript release factor OS=Homo sapiens GN=PTRF PE=1 SV=1	43.4	53.5	1	4.6	0.81
COR1C_HUMAN	Coronin-1C OS=Homo sapiens GN=CORO1C PE=1 SV=1	53.2	51.8	1	3.4	0.81
TIM50_HUMAN	Mitochondrial import inner membrane translocase subunit TIM50 OS=Homo sapiens GN=TIMM50 PE=1 SV=2	39.6	55.4	2	7.6	0.81
ACSL3_HUMAN	Long-chain-fatty-acid--CoA ligase 3 OS=Homo sapiens GN=ACSL3 PE=1 SV=3	80.4	103.3	4	7.5	0.79
RL11_HUMAN	60S ribosomal protein L11 OS=Homo sapiens GN=RPL11 PE=1 SV=2	20.2	36	1	7.9	0.79
CAH12_HUMAN	Carbonic anhydrase 12 OS=Homo sapiens GN=CA12 PE=1 SV=1	39.4	85.4	2	13	0.79
EIF3E_HUMAN	Eukaryotic translation initiation factor 3 subunit E OS=Homo sapiens GN=EIF3E PE=1 SV=1	52.2	44.2	1	2.9	0.78
K1C10_HUMAN	Keratin, type I cytoskeletal 10 OS=Homo sapiens GN=KRT10 PE=1 SV=6	58.8	140.3	5	9.4	0.78
UGGG1_HUMAN	UDP-glucose:glycoprotein glucosyltransferase 1 OS=Homo sapiens	177.1	37.3	1	0.9	0.77

	GN=UGGT1 PE=1 SV=3					
VAPB_HUMAN	Vesicle-associated membrane protein-associated protein B/C OS=Homo sapiens GN=VAPB PE=1 SV=3	27.2	34.9	1	5.8	0.75
SC22B_HUMAN	Vesicle-trafficking protein SEC22b OS=Homo sapiens GN=SEC22B PE=1 SV=4	24.6	38.1	1	5.6	0.74
PTGES_HUMAN	Prostaglandin E synthase OS=Homo sapiens GN=PTGES PE=1 SV=2	17.1	43.1	1	6.6	0.72
DIC_HUMAN	Mitochondrial dicarboxylate carrier OS=Homo sapiens GN=SLC25A10 PE=1 SV=2	31.3	39.6	1	8.4	0.72
UBQL1_HUMAN	Ubiquilin-1 OS=Homo sapiens GN=UBQLN1 PE=1 SV=2	62.5	69.6	2	5.9	0.71
SF3B1_HUMAN	Splicing factor 3B subunit 1 OS=Homo sapiens GN=SF3B1 PE=1 SV=3	145.7	64.9	2	3.4	0.70
PSB6_HUMAN	Proteasome subunit beta type-6 OS=Homo sapiens GN=PSMB6 PE=1 SV=4	25.3	34.1	1	3.8	0.70
ITA3_HUMAN	Integrin alpha-3 OS=Homo sapiens GN=ITGA3 PE=1 SV=5	116.5	81.6	2	2.6	0.69
ESYT1_HUMAN	Extended synaptotagmin-1 OS=Homo sapiens GN=ESYT1 PE=1 SV=1	122.8	83.2	3	3.6	0.68
GLSK_HUMAN	Glutaminase kidney isoform, mitochondrial OS=Homo sapiens GN=GLS PE=1 SV=1	73.4	31.4	1	2.5	0.67
PSMD1_HUMAN	26S proteasome non-ATPase regulatory subunit 1 OS=Homo sapiens GN=PSMD1 PE=1 SV=2	105.8	50.5	2	4	0.65
DDX42_HUMAN	ATP-dependent RNA helicase DDX42 OS=Homo sapiens GN=DDX42 PE=1 SV=1	102.9	33.5	1	1.4	0.65
TGM2_HUMAN	Protein-glutamine gamma-glutamyltransferase 2 OS=Homo sapiens GN=TGM2 PE=1 SV=2	77.3	68.7	2	4.2	0.65
AT1A2_HUMAN	Sodium/potassium-transporting ATPase subunit alpha-2 OS=Homo sapiens GN=ATP1A2 PE=1 SV=1	112.2	88.9	1	1.8	0.64
ROA0_HUMAN	Heterogeneous nuclear ribonucleoprotein A0 OS=Homo sapiens GN=HNRNPA0 PE=1 SV=1	30.8	67.6	2	7.5	0.62
TOP2B_HUMAN	DNA topoisomerase 2-beta OS=Homo sapiens GN=TOP2B PE=1 SV=3	183.2	34.9	1	0.7	0.61
PRS10_HUMAN	26S protease regulatory subunit 10B OS=Homo sapiens GN=PSMC6 PE=1 SV=1	44.1	101.8	3	10.8	0.60
TPD52_HUMAN	Tumor protein D52 OS=Homo sapiens GN=TPD52 PE=1 SV=2	24.3	37.7	1	6.7	0.59
THOC4_HUMAN	THO complex subunit 4 OS=Homo sapiens GN=ALYREF PE=1 SV=3	26.9	71.9	3	15.2	0.58
DEST_HUMAN	Destrin OS=Homo sapiens GN=DSTN PE=1 SV=3	18.5	37	1	8.5	0.56
NAA15_HUMAN	N-alpha-acetyltransferase 15, NatA auxiliary subunit OS=Homo sapiens GN=NAA15 PE=1 SV=1	101.2	36.6	1	1.7	0.53
RSMB_HUMAN	Small nuclear ribonucleoprotein-associated proteins B and B' OS=Homo sapiens GN=SNRPB PE=1 SV=2	24.6	27.3	1	3.3	0.52
MYADM_HUMAN	Myeloid-associated differentiation marker OS=Homo sapiens GN=MYADM PE=1 SV=2	35.3	60.7	1	7.1	0.44

[1] UniProtKB accession numbers; [2] Molecular weight; [3] Mascot score; [4] Number of identified peptides; [5] Sequence coverage; [6] Median of the measured iTRAQ ratios.

CHAPTER 7. REFERENCES

American Cancer Society. Cancer Facts & Figures 2016. *Cancer Facts Fig. 2016* 1–9 (2016).

Bai, L., Lin, G., Sun, G., Liu, Y., Huang, X., Cao, C., Guo, Y., Xie, C. Upregulation of SIRT6 predicts poor prognosis and promotes metastasis of non-small cell lung cancer via the ERK1 / 2 / MMP9 pathway. *Oncotarget.* 7, 40377–40386 (2016).

Boyadjiev, S. A., Fromme, J. C., Ben, J., Chong, S. S., Nauta, C., Hur, D. J., Zhang, G., Hamamoto, S., Schekman, R., Ravazzola, M., Orci, L., Eyaid, W. Cranio-lenticulo-sutural dysplasia is caused by a SEC23A mutation leading to abnormal endoplasmic-reticulum-to-Golgi trafficking. *Nature Genet*. 38, 1192-1197 (2006).

Britz SJ, Prasad PV V, Moreau R a, Allen LH, Kremer DF, Boote KJ. Influence of growth temperature on the amounts of tocopherols, tocotrienols, and gamma-oryzanol in brown rice. *J Agric Food Chem*. 55, 7559-7565 (2007).

Dapar, M., Garzon, J., Demayo, C. Cytotoxic activity and Antioxidant Potentials of hexane and Methanolextracts of IR64 Rice bran against Human Lung (A549) and Colon (HCT116) Carcinomas. *Int Res J Biological Sci*. 2, 19-23 (2013).

George, B., Horn, D., Bayo, P., Zaoi, K., Flechtenmacher,C. et al. Regulation and function of Myb-binding protein 1A (MYBBP1A) in cellular senescence and pathogenesis of head and neck cancer. *Cancer Letters* 358, 191–199 (2015).

Goyal, S., Gupta, N., Chatteriee, S., Nimesh, S. Natural plant extracts as potential therapeutic agents for the treatment of cancer. *Curr Top Med Chem.*(2016).

Hirsch, G., Parisi, M., Martins, L., Andrade, C., Bernabé-Tuana, F., Guma, F. γ-oryzanol reduces caveolin-1 and PCGEM1 expression, markers of agressiveness in prostate cancer cells. *Prostate.* 75, 783-97 (2015).

Huang C.J., Godber J.S.. Potential functionality and digestibility of oryzanol as determined using in vitro cell culture models. (2003).

Jemal, A., Siegel, R., Ward, E., Hao, Y., Xu, J., Thun, M. J. Cancer statistics, 2009. *Cancer J Clin*. 59, 225−49 (2009).

Kiessling, M., Curioni-Fontecedro, A., Samaras, p., Lang, S., Scharl, M., Aguzzi, A., Oldrige, D., Maris, J., Rogler, G. Targeting the mTOR complex by everolimus in NRAS mutant neuroblastoma. *Plos One*. 11, doi:10.1371/journal.pone.0147682 (2016).

Kim, J.E., Chen, J., Lou, Z.DBC1 is a negative regulator of SIRT1. *Nature*. 451, 583-586 (2008).

Kim, H.W., Kim, J.B., et al. Evaluation of γ-oryzanol content and composition from the grains of pigmented rice-germplasms by LC-DAD-ESI/MS. *BMC Res. Notes*. 6, 149 (2013).

Kim HW, Kim JB, Cho S-M, et al. Characterization and quantification of γ-oryzanol in grains of 16 Korean rice varieties. *Int J Food Sci Nutr*. 66, 166-174 (2015).

Klongpityapong, P., Supabphol, R., Supabphol, A. Antioxidant effects of gamma-oryzanol on prostate cancer cells. *Asian Pac J Cancer Prev*. 14, 5421-5425 (2013).

Korpal, M., Ell, B., Buffa, F., Ibrahim, T., Blanco, M., Celia-Terrassa, T., Mercatali, L., Khan, Z., Goodarzi, H. et al. Direct targeting of SEC23A by miR-200s influences cancer cell secretome and promotes metastatic colonization. *Nat Med.* 17, 1101-1108 (2012).

Krypuy, M., Newnham, G. M., Thomas, D. M., Conron, M. & Dobrovic, A. High resolution melting analysis for the rapid and sensitive detection of mutations in clinical samples: KRAS codon 12 and 13 mutations in non-small cell lung cancer. *BMC Cancer*.6, 295 (2006).

Kumamoto, T., Seki, N., Mataki, H., Mizuno, K., Kamikawaji, K., Samukawa, T. et al. Regulation of TPD52 by antitumor microRNA-218 suppresses cancer cell migration and invasion in lung squamous cell carcinoma. *Int. J. Oncol*. 1870–1880 (2016).

Lee, S., Kim, J., Cho, E. & Youn, H. A nucleocytoplasmic malate dehydrogenase regulates p53 transcriptional activity in response to metabolic stress. *Cell Death Differ*. 16, 738–748 (2009).

Li, L., Su,n H., Liu, X., Gao, S., Jiang, H., Hu, X., et al. Down-regulation of NDUFB9 promotes breast cancer cell proliferation, metastasis by mediating mitochondrial metabolism. *Plos One.* 10, 1–15 (2015).

Li, Y., Wang, H., Zheng, S. Rab1 GTPases as oncogenes. *Aging*. 7, 897-898 (2015).

Mandak, E., Nyström, L. The effect of in vitro digestion on steryl ferulates from rice (Oryza sativa L.) and other grains. *J. Agric. Food Chem.*60, 6123–6130 (2012).

Martín-Bernabé, A., Cortés, R., Lehmann, S. G., Seve, M., Cascante, M., Bourgoin-Voillard, S. Quantitative proteomic approach to understand metabolic adaptation in non-small cell lung cancer. *J Proteome Res*. (2014).

Ming, Z., Jiang, M., Li, W., Fan, N., Deng, W., Zhong, Y. et al. Bioinformatics analysis and expression study of fumarate hydratase in lung cancer. *Thorac. Cancer.* 5, 543–549 (2014).

Ming, M., Han, W., Zhao, B., Sundaresan, N., Deng, C., Gupta, M., He, Y. SIRT6 promotes COX-2 expression and acts as an oncogene in skin cancer. *Cancer Res.* 7, 5925–5933 (2014).

Mosmann, T. Rapid Colorimetric Assay for Cellular Growth and Survival : Application to Proliferation and Cytotoxicity Assays. *J Immunol Methods.* 65, 55–63 (1983).

Ono, W., Hayashi1, Y., Yokoyama, W., Kuroda, T., Kishimoto, . et al. The nucleolar protein Myb-binding protein 1A (MYBBP1A) enhances p53 tetramerization and acetylation in response to nucleolar disruption. *J Biol Chem*, 289, 4928-4940 (2014).

Ostrem, J.M., Peters, U., Sos, M. L., Wells, J.A., Shokat, K.M. K-Ras(G12C) inhibitors allosterically control GTP affinity and effector interactions. *Nature.* 503, 548–551 (2013).

Owen, H., Elser, M., Cheung, E., Gersbach, M., Kraus, W., Hottiger, M. MYBBP1A is a novel repressor of NFκB. *J Mol Biol.* 366, 725–736 (2007).

Pal, H.C., Hunt, K.M., Elmets, C.A., Agaf, F. Phytochemicals for the management of melanoma. *Mini Rev Med Chem.*(2016).

Patel, N.; Naik, S. N. Gamma- oryzanol from rice bran oil – A review. *J. Sci. Ind. Res.* 63, 569-578 (2004).

Perrera, C., Colombo, R., Valsasina, B., Carpinelli, P., Troiani, S. et al. Identification of Myb-binding Protein 1A (MYBBP1A) as a Novel Substrate for Aurora B Kinase. *J Biol Chem*. 285, 11775–11785 (2010.

Petkovic, M., Jemaiel, A., Daste, F., Specht, C., Izeddin, I., Vorkel, D. et al. The SNARE Sec22b has a non-fusogenic function in plasma membrane expansion. *Nat. Cell Biol*. 16, 434–44 (2014).

Polyakova, O., Borman, S., Grimley, R., Vamathevan, J., Hayes, B., Solari, R. Identification of novel interacting partners of sirtuin6. *Plos one.*7, e51555 (2012).

Riely, G. J., Marks, J. & Pao, W. KRAS Mutations in Non-Small Cell Lung Cancer. *Proc. Am. Thorac. Soc.*6, 201–205 (2009).

Riss, T.; Moravec, R.; Niles, A.; Benink, H.; Worzella, T.; Minor, L. Cell Viability Assays. Sittampalam GS, Coussens NP, Nelson H, et al., editors. *Assay Guidance Manual* [Internet]. Bethesda (MD): Eli Lilly & Company and the National Center for Advancing Translational Sciences; 2004 [Cited April 2016]. Available from: http://www.ncbi.nlm.nih.gov/books/NBK144065/.

Sakai, S., Murata, T., Tsubosaka, Y., Ushio, H., Hori, Ozaki, H. γ-oryzanol reduces adhesion molecule expression in vascular endotelial cells via suppression of nuclear factor- κB activation. *J. Agric. Food Chem*. 60, 3367−3372 (2012).

Sohail, M.; Rakha, A.; Butt, M.S.; Iqbal, M.J.; Rashid, S. Rice bran nutraceutics: a comprehensive review. *Food Sci Nutr.* 1040-8398 (2016).

Szcześniak, K. A., Ostaszewski, P., Ciecierska, A. & Sadkowski, T. Investigation of nutriactive phytochemical - gamma-oryzanol in experimental animal models. *J. Anim. Physiol. Anim. Nutr.* (Berl). 100 (2015).

Unwin, R., Griffiths, J., Whetton, A. Simultaneous analysis of relative protein expression levels across multiple samples using iTRAQ isobaric tags with 2D nano LS-MS/MS. *Nature protocols.* 5, 1574-1582 (2010).

Wheeler, D.L., Iida,M., Dunn, E.F. The role of SRC in solid tumors. *Oncologist*.14, 667-678 (2009).

Xu Z, Godber JS. Antioxidant activities of major components of γ-oryzanol from rice bran using a linoleic acid model. *J Am Oil Chem Soc*. 78, 645-649 (2001).